Joule

CellPress

Article

A comparative energy and costs assessment and optimization for direct air capture technologies

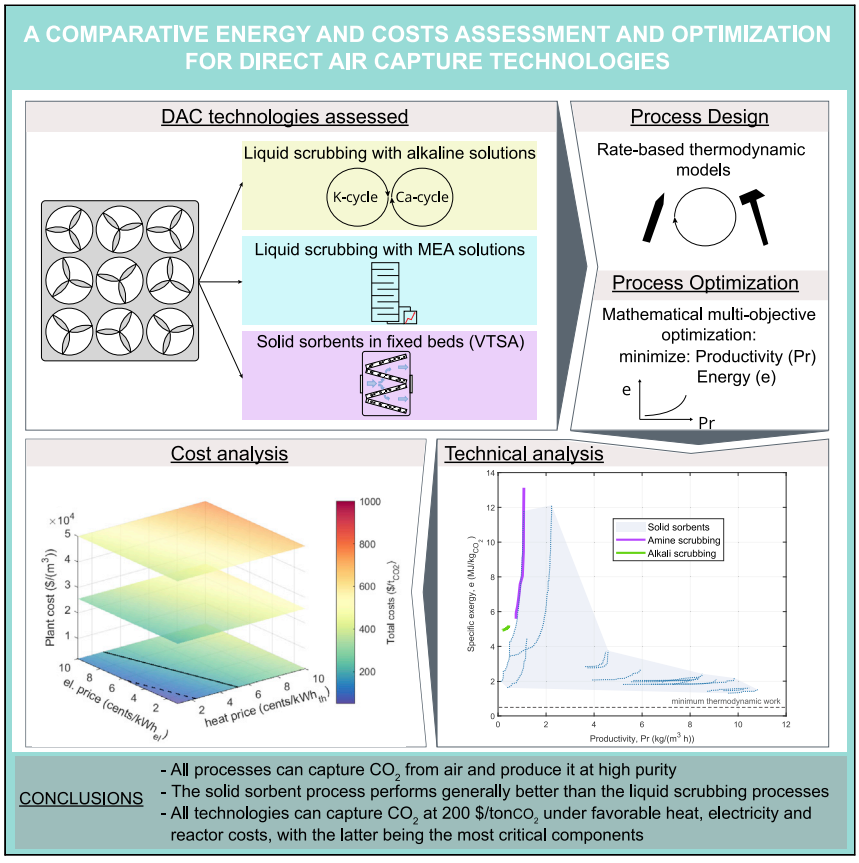

The direct extraction of CO_2 from air—or direct air capture (DAC)—at gigatons scale will likely be a necessary measure to keep global warming below 1.5°C. Due to DAC's novelty, a large potential exists for reducing energy and cost requirements. With this contribution, we provide a detailed analysis of the two main technological routes, aqueous- and solid-based processes, and compare their performance on the grounds of energy, productivity, and costs.

Francesco Sabatino, Alexa Grimm, Fausto Gallucci, Martin van Sint Annaland, Gert Jan Kramer, Matteo Gazzani

m.gazzani@uu.nl

Highlights

Three DAC processes were compared on the basis of exergy demand and productivity

Solid sorbent-based processes perform better than solvent-based processes

CO_2 capture costs below 200 $/t$CO_2$ are achievable for all technologies

Adsorption/desorption kinetics and H_2O affinity strongly affect solid sorbent process

Sabatino et al., Joule 5, 2047–2076
August 18, 2021
https://doi.org/10.1016/j.joule.2021.05.023

Joule

CellPress

Article

A comparative energy and costs assessment and optimization for direct air capture technologies

Francesco Sabatino,[1,3] Alexa Grimm,[2,3] Fausto Gallucci,[1] Martin van Sint Annaland,[1] Gert Jan Kramer,[2] and Matteo Gazzani[2,4,*]

SUMMARY

This work provides a comparative technical assessment of three technologies for CO_2 removal from air: two aqueous-scrubbing processes and one solid sorbent process. We compute productivity and exergy and energy consumption using process simulations and mathematical optimization. Moreover, we evaluate the cost range and discuss the challenges for large-scale deployment. We show that all technologies can provide high-purity CO_2 and that the solid-based process has the potential to offer the best performance, owing to an exergy demand of 1.4–3.7 $MJ.kg_{CO_2}^{-1}$ and a productivity of 3.8–10.6 $kg_{CO_2}.m^{-3}.h^{-1}$. Translating productivity and energy into cost of CO_2 capture via a simple model, we show that the capital cost is the main cost driver. All technologies have the potential to operate below 200 $\$.ton_{CO_2}^{-1}$ under favorable, yet realistic, energy and reactor costs. The solid-sorbent process achieves this under a broader range of conditions and is less dependent on the installation cost when a high mass transfer is achieved.

Context & scale

Artificial removal of CO_2 from the atmosphere will be pivotal for the realization of CO_2-net-zero plans and policies. Among the few available solutions, the direct extraction from air—or direct air capture (DAC)—features the highest removal potential. Although energy and economic expenditure are high, DAC is still in its infancy, and a large potential exists for its optimization. To scale up the production, the different processes should be consistently evaluated, their design and operation optimized, and the needs for further development identified. Surprisingly, this is missing in the literature. In this study, we discuss the optimal process design and performance for the main DAC technologies, starting from publicly available unit designs and data and by using advanced simulation tools. Moreover, we identify the open challenges that need addressing and compute the CO_2 capture cost as a function of energy and equipment costs, showing the combinations that would allow for cheaper DAC units.

INTRODUCTION

Limiting global warming at 2°C, and possibly at 1.5°C, is of paramount importance to keep the results of climate change manageable. The Paris agreement that was signed in 2016 was designed for this purpose; however, its non-binding and unenforceable nature has yet to trigger the required set of actions for successful 1.5°C policies. Hence, it should not come as a surprise that the Intergovernmental Panel on Climate Change (IPCC) expects the global warming to be higher than the 1.5°C target.[1] Avoiding an overshoot of 1.5°C would likely require a 45% reduction of the net anthropogenic carbon dioxide (CO_2) emissions from 2010 levels by 2030 and reaching net zero around 2050.[2] Reduction measures will be key to achieve this abatement and, among them, carbon capture and storage (CCS) will play an important role in reducing the emissions associated with the continuous use of fossil fuels. This is particularly relevant for industrial processes, such as cement and steel production and carbon-based chemical production. Not surprisingly, all the pathways consistent with a 1.5°C temperature increase are dependent, to some extent, on the deployment of negative emissions technologies (NETs)[2] that actively remove CO_2 from the atmosphere. Among the potential NET solutions, direct air capture (DAC), which refers to the extraction of CO_2 from air through an artificial contactor, can be engineered, and therefore possesses a very high mitigation potential.[3] However, DAC is a relatively novel process that is in the early stages of development and commercialization[4]; many questions remain to be answered and the improvement potential is high.

Gas separation is a pillar of chemical engineering, and many processes exist that can be used for such scope. Several mature gas-separation technologies make use of

physical processes; however, because of the ultra-diluted concentration of CO_2 in air, they are not good candidates for DAC.[5] Also, strong affinity for CO_2 is required for its effective separation from air.[6]

Currently, there are a few processes that can be used for DAC. Zeman and Lackner were the first to describe a process in which CO_2 is extracted from air through wet scrubbing with an aqueous alkali hydroxide.[7] This DAC system consists of two cycles. In the first one, sodium or potassium hydroxide reacts with CO_2 to produce carbonates, which are soluble in water. In the second cycle, the carbonates are causticized with lime ($Ca(OH)_2$) resulting in the precipitation of $CaCO_3$, which is then heated above 900°C to release CO_2. This concept was further developed by Baciocchi et al.,[8] who provided the first conceptual design based on mass and energy balances. Several issues were pointed out; the most important being the high and essentially unavoidable energy demand of the solvent regeneration. Later, in a report by the American Physical Society (APS) alkali scrubbing was selected as the benchmark process for DAC and a cost of about $600 per ton of captured CO_2 was estimated.[9] However, other estimates based on different absorption unit design are lower. Due to the concentration of CO_2 in the atmosphere, large volumes of air have to be processed to capture a relevant amount of CO_2. Hence, efficient air contact with the solvent is extremely important. This is where the DAC company Carbon Engineering has focused its early development efforts. By using a different design of an absorption unit, tailor-made for air capture applications, Holmes and coworkers estimated that the total costs of the air contactor alone (that is, neglecting the costs for the regeneration of the solvent) could be drastically reduced from the 240 $/ton$_{CO_2}$ assessed by the APS[9] to 60 $/ton$_{CO_2}$.[10] The air contactor[11] and some of the units involved in the solvent regeneration[12] have also been tested at pilot scale with promising results, prompting Carbon Engineering to plan the construction of a 1 Mton$_{CO_2}$/year DAC plant. However, the major drawbacks related to the caustic recovery of the alkali hydroxide have not been overcome, and alternative regeneration techniques show limited potential.[13]

An alternative absorption-based DAC process has been described by Custelcean et al.[14] In this process CO_2 is extracted from air by an aqueous solution of amino acids, such as glycine or sarcosine, yielding the corresponding bicarbonate salts. The amino acid is subsequently recovered by crystallization of the carbonate anions with a bis-iminoguanidine solid. Finally, the carbonate crystals are decomposed at temperatures between 60°C and 120°C, thus releasing high-purity CO_2. While the temperature required for the regeneration of the solvent is lower compared with the alkali scrubbing process, the energy demand of the process proposed by Custelcean et al. is higher.[15] Indeed, amino acid solvents provide fast absorption kinetics but low cyclic capacity.

Surprisingly, liquid scrubbing via alkanolamines (e.g., monoethanolamine [MEA]) has been hardly considered for applications in DAC. In fact, amine scrubbing is the benchmark technology for post-combustion CO_2 capture and has been applied in hundreds of gas-separation processes.[16] In its basic form, the process consists of the extraction of CO_2 from (flue) gases near ambient temperature with an aqueous solution of amines, followed by regeneration of the solvent through stripping at about 120°C. Alkanolamines have a high affinity for CO_2, which is enough for CO_2 capture from air.[17] Despite this, liquid scrubbing with MEA has only very recently been assessed as an option for DAC. Barzagli et al. have conducted an experimental screening of amine-based solutions as solvents for DAC.[18] Aqueous primary amines appeared to be the best candidates, with MEA capturing 87.3% of CO_2 from air in a

[1]Department of Chemical Engineering and Chemistry, Technische Universiteit Eindhoven, 5600 MB Eindhoven, the Netherlands

[2]Utrecht University, Copernicus Institute of Sustainable Development, Princetonlaan 8a, 3584 CB Utrecht, the Netherlands

[3]These authors contributed equally

[4]Lead contact

*Correspondence: m.gazzani@uu.nl

https://doi.org/10.1016/j.joule.2021.05.023

24-hour period. Kiani et al. have carried out a simulation study and economic evaluation in Aspen Plus, adapting the conventional MEA-based absorption process for the capture of CO_2 from air.[19] The total estimated cost for this process was 1,690 $/ton$_{CO_2}$ in the base case. The high cost is substantially due to the high capital expenditure required for the absorption column, but Kiani et al. have adopted a conventional packed column as absorber, which is not an optimal design for DAC. In fact, they report that using a cooling tower inspired system, as the one designed by Carbon Engineering, could reduce the cost of the absorber by 83%. However, it remains that amine scrubbing requires great amounts of low-grade heat for regeneration, and that amines are generally corrosive and toxic and degrade over time due to oxidation.[20]

These disadvantages can partly be overcome through immobilization of amines on solid supports. By exchanging H_2O with a solid support with lower heat capacity, the amount of energy required to regenerate the amines can be reduced significantly.[21] Moreover, degradation and corrosion in supported amine are less of a problem.[22] In fact, amine-functionalized sorbents are currently receiving significant attention in the DAC scientific community[6,23]; early DAC companies adopted them for their commercial processes. Among them, Climeworks proposed porous granulates modified with amines applied in vacuum-pressure temperature swing adsorption (VTSA) cycles.[24] In this process, unloaded sorbent material is contacted with air to capture carbon dioxide at ambient condition; subsequently, the unit is evacuated to a pressure in the range of 20–400 mbar and heated to a temperature of 80°C–130°C to desorb CO_2.[25] The combination of vacuum and temperature allows for a higher cyclic capacity and therefore limits the amount of sorbent needed. Finally, the unit is repressurized and cooled down to ambient conditions. Climeworks and Global Thermostat are two established startups developing and commercializing such DAC processes, with multiple pilot plants already running or being built.[26] In addition to the specific sorbents, which differ in composition and structure, the two companies have opted for different contactors. Whereas Climeworks employs air-filter-like structures,[27] Global Thermostat uses honeycomb monoliths.[28] In both cases, a VTSA cycle is used as process.

Another class of solid materials that has shown promising performances both as sorbents[29,30] and supports[31,32] are metal-organic frameworks (MOFs). MOFs are hybrid structures with metal nodes linked by organic bridges in bi- or three-dimensional crystalline structures. Their large design space and versatility have made MOFs good candidates for various gas-separation applications; surface area and pore characteristics can be tailor-tuned, and open metal sites allow for additional functional groups. On the other side, production and commercialization of MOFs at large scale is still an unsolved challenge.[33]

An important point that need attention when considering solid sorbents is the behavior with respect to water adsorption. Depending on the ambient conditions and the solid characteristics, H_2O can affect the adsorption of CO_2 and therefore the process productivity and energy requirements. More specifically, it is important to obtain high quality experimental data and implement a suitable model for water competitive or cooperative adsorption.[22,34] So far, this point has largely been overlooked in open scientific literature.

We can conclude that two DAC technologies stand out in light of the scale at which they have been deployed and the technological readiness they have achieved. These two technologies are wet scrubbing with aqueous alkali hydroxide solutions[12] and VTSA on supported sorbents.[35] Moreover, we argue that MEA scrubbing should

also be regarded as an equally ready DAC technology. These processes have different advantages and disadvantages. Liquid scrubbing is a continuous process that can take advantage of mature and inexpensive components. However, the regeneration is costly and complex, especially for alkali solvents. The VTSA process is simpler in principle, since the CO_2 capture and the sorbent regeneration are carried out in the same unit. Moreover, the regeneration of the sorbent takes place at low temperature. On the other hand, the process is not as mature as liquid scrubbing, the sorbent stability is still an issue and achieving high CO_2 purity requires customized and more energy-demanding cycles.

Choosing between these two approaches and prioritizing their research and development is therefore not trivial; the projected cost of both technologies once deployed at large scale has been estimated to be around \$100 per ton of CO_2 captured[26]; though this value might be too optimistic, \$200 per ton of CO_2 is a likely target that DAC companies are pursuing. However, it remains unclear what specific actions are needed to be taken to get there and where improvements are most needed.

With this extensive work we provide a thorough process analysis for aqueous- and solid-based DAC technologies. We do this by coupling advanced rate-based process modeling with mathematical multi-objective process optimization. For the thermodynamic modeling, we use Aspen Plus for liquid solvents, and a state-of-the-art in-house code for fixed bed cycles with solid sorbents.[36] For the process optimization, we directly connect the first-principles rate-based models to Matlab, where we use suitable mathematical algorithms to identify the optimal design. As a result, we are able to compute the specific energy consumption (in MJ $kg_{CO_2}^{-1}$) and CO_2 productivity (in $kg_{CO_2}\ m^{-3}\ h^{-1}$) starting from thermodynamic models of specific reactor designs, which are adopted from existing pilot plants. These two key performance indicators (KPIs) provide the required input for a simplified cost model that, despite its simplicity, is able to clearly map the main contributions to the total specific cost (in \$ $kg_{CO_2}^{-1}$) and the directions to follow for further improvements; e.g., benefits from reduction in fixed costs versus reduction in operating costs. When comparing with the existing literature, although a few techno-economic analyses of DAC have been published, they either rely on simple process models,[37] or on energy assumptions from literature[26,38] or analyze a single process.[19,39–41] In addition, here we consider the presence of water and its co-adsorption. Accordingly, this work advances compared with existing literature as it (i) provides a detailed model-based comparison of the key DAC processes, (ii) assesses the potential of each DAC process via process models and optimization, (iii) identifies the main weak points of the selected technologies, thus providing input for future R&D, and (iv) quantifies how process/material improvements could enhance the performance.

This work is organized as follows. In process schemes and methodology, we describe the considered DAC processes and the modeling approach adopted for their analysis. This is complemented by an exhaustive supplemental information document. In multi-objective optimization, we describe the process optimization and in economic evaluation, the economic analysis methodology. In results and discussion, we present the main results. Finally, in processes comparison and economic evaluation and conclusions we discuss the results and summarize the main conclusions, respectively.

Process schemes and methodology

Alkali scrubbing

The alkali-scrubbing process is shown in Figure 1. The process has been thoroughly discussed in past literature[7,8,12]; however, it has never been systematically

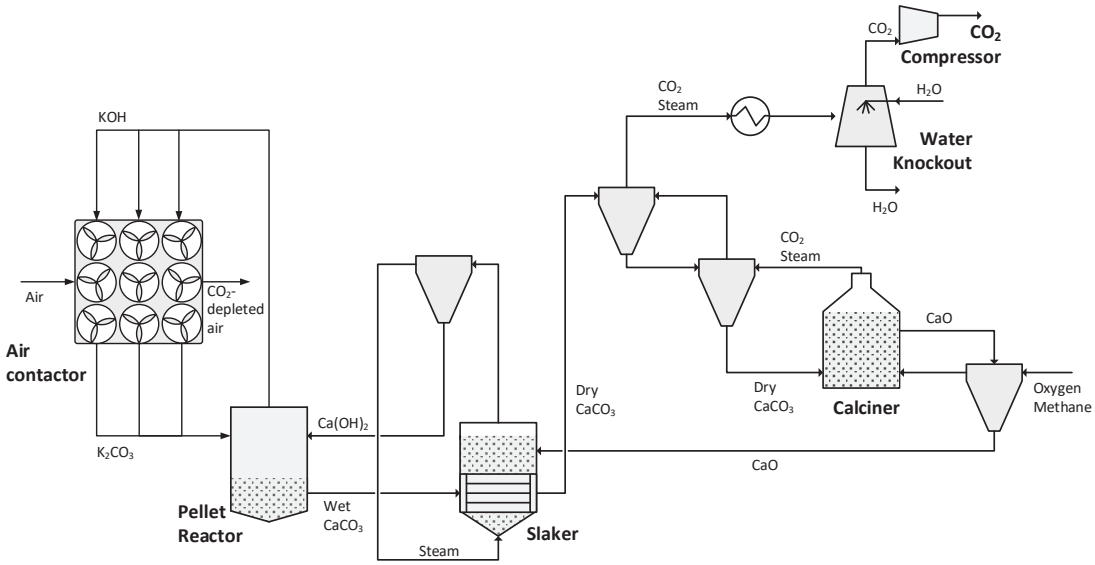

Figure 1. Schematic representation of the alkali-scrubbing DAC process

optimized. Here, we shortly discuss the process features, especially in light of modeling and optimization; the reader can refer to literature or the supplemental information for more details on the process units.

In the alkali scrubbing, CO_2 is captured in a dedicated air contactor unit, where it is absorbed in an aqueous solution of KOH in the form of K_2CO_3. The K_2CO_3 solution is regenerated by forming calcium carbonate, which is then fed to a calciner and decomposed to CaO and CO_2. In this work, the whole process is modeled using Aspen Plus V11, which allows for precise computation of relevant thermodynamics via the electrolyte NRTL method, while also providing a reliable rate-based model (available within RadFrac).

The absorption mechanism of carbon dioxide in alkaline solutions is well known and takes place through a two-step process[42]:

$$CO_{2(aq)} + OH^- \rightleftharpoons HCO_3^- \quad \text{(Equation 1)}$$

$$HCO_3^- + OH^- \rightleftharpoons CO_3^{2-} + H_2O \quad \text{(Equation 2)}$$

The rate-limiting step of the absorption mechanism is represented by Equation 1. This mechanism is common to all alkali hydroxide sorbents, but it is reported that KOH provides the fastest kinetics.[11,43] In our simulations, we consider the air contactor design developed by Carbon Engineering,[10] who adapted commercial cooling tower technologies to fit liquid scrubbing for DAC application (see supplemental information for additional details). Notably, such original units are devised to efficiently bring very large quantities of ambient air into contact with water. The kinetics for the absorption reactions have been adapted from the work of Pinsent et al.,[44] while pressure drops are estimated using the built-in correlations in Aspen Plus for the selected packing.

The regeneration of the solvent and collection of CO_2 are carried out through a calcium-based thermo-chemical cycle, a process that has been adapted from the Kraft pulping widely used in the paper industry.[5] The CO_2-rich solution coming from the

air contactor is fed to the pellet reactor, where K_2CO_3 is converted back to KOH through causticization with lime according to the following reaction:

$$K_2CO_{3(aq)} + Ca(OH)_{2(aq)} \rightleftharpoons 2KOH_{(aq)} + CaCO_{3(s)} \quad \text{(Equation 3)}$$

Calcium carbonate has an extremely low solubility in water and, therefore, precipitates and it is easily separated from the liquid phase, which is sent back to the air contactor. However, the rate of reaction in Equation 3 is driven by the concentration of Ca^{2+} ions, which is low in highly alkaline solutions due to the low solubility of $Ca(OH)_2$ in these conditions.[7] This could be an issue, as the CO_2-rich solution coming from the air contactor still contains a considerable amount of KOH, but it can be tackled by having calcium hydroxide as the limiting reactant and by long residence times in the pellet reactor.[12,45]

The wet $CaCO_3$ particles are collected from the bottom of the pellet reactor and are dried and preheated before being fed to the calciner, where CO_2 is released upon decomposition of calcium carbonate:

$$CaCO_{3(s)} \rightarrow CaO_{(s)} + CO_{2(g)} \quad \text{(Equation 4)}$$

The final step of the regeneration cycle is carried out by the slaker, where the hydration of CaO to $Ca(OH)_2$ takes place according to:

$$CaO_{(s)} + H_2O_{(g)} \rightarrow Ca(OH)_{2(s)} \quad \text{(Equation 5)}$$

The design of the regeneration process and the performances of the unit operations comprising it have been based upon the data published by Keith et al.[12] Key parameters used for modeling the alkali-scrubbing process are reported in Table S6.

Amine scrubbing

The amine-scrubbing process differs from the alkali scrubbing in the regeneration section, where it is considerably simpler. The process layout is shown in Figure 2.

The air contactor designed by Carbon Engineering is adopted also in this case, as it provides a clear advantage over conventional absorption columns. The chemical absorption of CO_2 in the aqueous MEA solution takes place via reaction with the hydroxide ion (Equations 1 and 2) and according to the following reactions[46]:

$$MEA + CO_{2(aq)} + H_2O \rightleftharpoons MEACOO^- + H_3O^+ \quad \text{(Equation 6)}$$

$$MEA + H_3O^+ \rightleftharpoons MEAH^+ + H_2O \quad \text{(Equation 7)}$$

As opposed to K_2CO_3, MEA has a relatively high vapor pressure, resulting in a considerable potential loss of solvent to the atmosphere. Additionally, MEA is a much more toxic substance and its impact on both humans and environment could be detrimental.[47] For this reason, a water-wash section has been employed to reduce the emissions of MEA. Additional details for this unit, which has been modeled following the same approach adopted for the air contactor, are reported in Table S1.

The rich solvent stream is first pumped to the stripper pressure and then split in two flows: the largest is preheated in conventional fashion by the lean/rich heat exchanger, while the other is kept cold and fed at the top of the stripper. With this arrangement, the vapor released from the hot rich stream is exploited to heat up the cold stream flowing from the top—a conventional practice in CO_2 capture from flue gases.[48] The rich solvent stream is regenerated through stripping with steam.

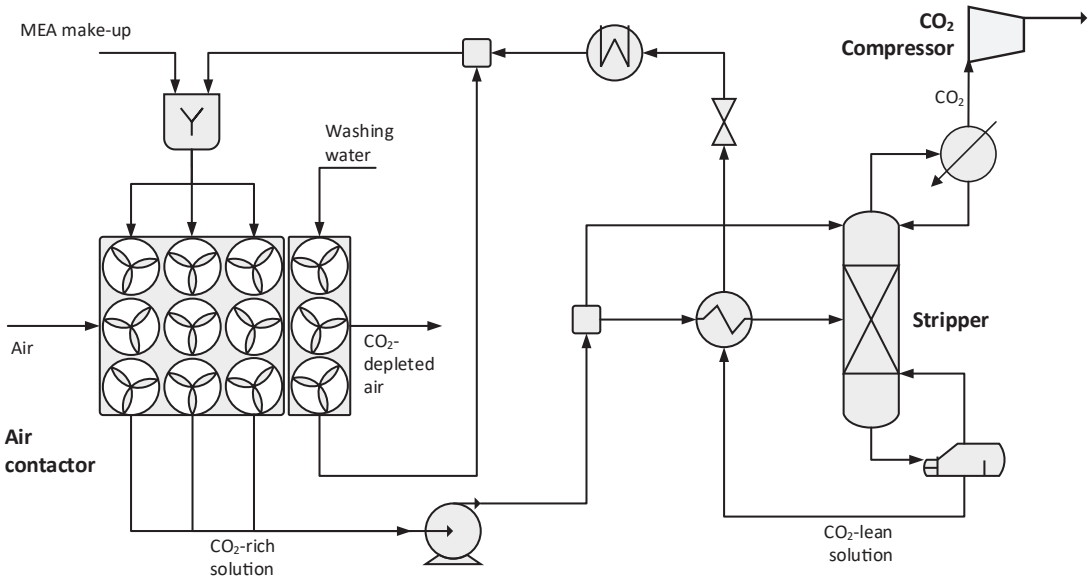

Figure 2. Schematic representation of the amine-scrubbing process

The properties of the liquid phase are evaluated with the unsymmetrical electrolyte NRTL method, while for the gas phase SRK equation of state is employed, a proven approach for amine systems.[49] The absorption reactions are implemented in the air contactor blocks through kinetically controlled reactions. The kinetic constants are as in the work of Amirkhosrow et al.,[50] who validated them under different operating conditions.

An equilibrium RadFrac block has been adopted to model the stripper, as the regeneration is usually carried out at conditions close to equilibrium. Details regarding the stripper are reported in Table S1.

Solid sorbent process

The simplified flow scheme of the adsorption process is shown in Figure 3. The plant consists essentially of the air contactor, controlling valves, a vacuum pump, and heat and cold supply. When looking at the details of the air contactor, the most mature version of the solid sorbent process is a cyclic process, where a single unit undergoes successively a loading (adsorption) and a regeneration (desorption) step at different pressures (pressure swing adsorption [PSA]). Because DAC treats air at ambient conditions and in very large flow rates, air compression is not a viable option, which leaves temperature and vacuum as the only regeneration drivers. Therefore, we consider a vacuum-temperature swing adsorption (VTSA) cycle, as illustrated with exemplary column status in Figure 4A. This cycle was synthesized to allow the production of CO_2 at high purity (dry) and consists of four different steps, i.e., (i) adsorption, (ii) purge, (iii) regeneration, and (iv) repressurization.

During the adsorption step, the air mixture enters the adsorber unit at ambient conditions. CO_2 (and H_2O) is selectively removed by the sorbent, and CO_2-lean air leaves the system. When the CO_2 front reaches the end of the bed this step is terminated. In order to increase the purity of CO_2, a preliminary heating step is introduced, whereby the air, mainly N_2, in the void space is removed. The sorbent is heated up to a temperature $T_1 < T_2$ by an external heating fluid, where 1 refers to the preheating and 2 refers to the heating step. At the same time, vacuum is

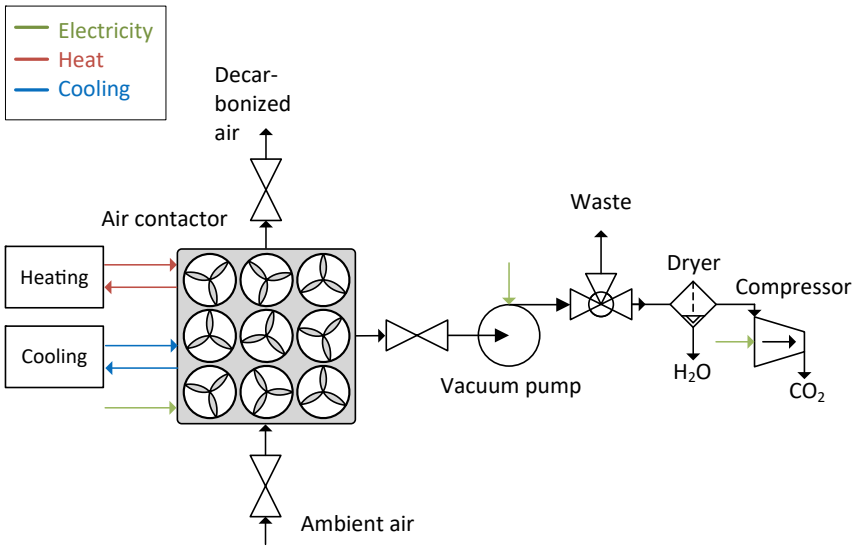

Figure 3. Simplified flowsheet of the capturing process using a solid sorbent

generated using vacuum pumps. Small amounts of CO_2 and H_2O are already desorbed during this step. During the main desorption step the sorbent is heated to the highest working temperature T_2, whereas the vacuum condition is maintained or even tightened. High-purity CO_2 in H_2O vapor is produced during this step and withdrawn from the column. Compared to the aqueous solution-based systems, lower temperatures at around 100°C are sufficient to regenerate the sorbent. Subsequently, the valve at the entrance is opened, and the ambient air streams in, which cools down the sorbent material and repressurizes the system until the column is back to the starting conditions.

As for the air contactor geometry, we have adopted the design described in patents of Climeworks.[52–54] In such a configuration, the air contactor, which is shown in Figure 4B, resembles an air ventilation system rather than a conventional adsorber column. The physical dimensions of the module, such as the length of the sorbent layer and the void space within the contactor, are set by choosing arbitrarily from the design range provided in several works.[52–54] Additional parameters used in the

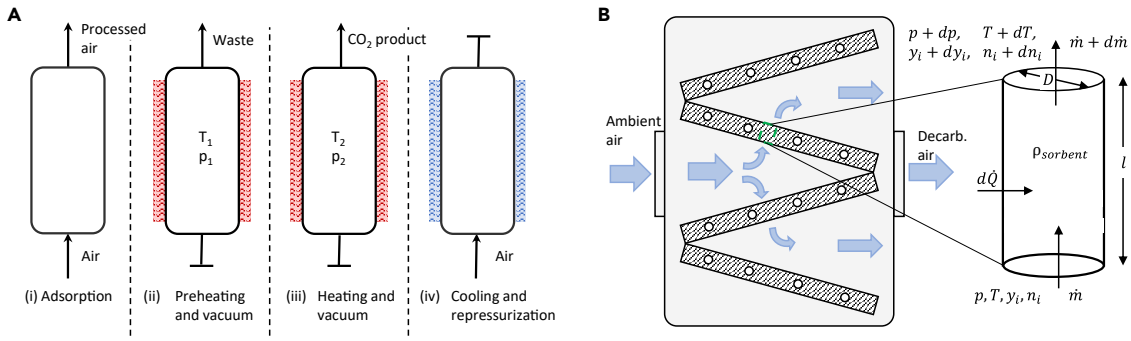

Figure 4. Representation of the adsorption process

(A and B) (A) The schematic design of the VTSA process, divided into four cycles. Note that here we use a column-type cycle representation for the sake of clarity. More information about the structure are given in Figure 3, and in (B) a schematic design of the air contactor unit comprising a number of plates containing the solid sorbent, similar to a design published in study conducted by Wurzbacher et al.[51]

process model are listed in Table S5. It is worth stressing that DAC companies may use different types of VTSA cycles and air contactor designs.

Extensive data is needed to model the adsorption process: from sorbent isotherms to transport parameters. We address them in the following section. Because adsorption-based DAC is not as established as liquid scrubbing, we provide more details than in alkali scrubbing and amine scrubbing.

Key for the process performance is indeed the sorbent. So far, several sorbents have been presented in the literature, but only few possess the minimum thermodynamic requirements for a successful DAC process. This can be clearly shown by plotting the CO_2 cyclic working capacity of the sorbent; i.e., the difference between the equilibrium CO_2 loading at adsorption and at desorption conditions, with respect to the desorption temperature (see Figure 5).

The sorbent selection in this work is therefore based on the following constraints: (i) cyclic capacity larger than zero when considering CO_2 partial pressure in the air for the adsorption and T_{max} = 120°C and p_{min} = 0.1 bar for the regeneration, and (ii) data availability in open scientific literature for relevant isotherms and sorbent physical properties. As a result, we selected four promising sorbents, which are highlighted in Figure 5, namely APDES-NFC,[52] Tri-PE-MCM-41,[55] MIL-101(Cr)-PEI-800,[31] and Lewatit VP OC 106.[34,56,57] It is worth noting that, because DAC is a relatively young application, experimental data are currently limited. On the one hand, data are missing about H_2O and N_2 adsorption under different conditions. On the other hand, multicomponent isotherms are not available to the best of our knowledge. More specifically, for the APDES-NFC and the Lewatit sorbent comprehensive experimental data for both water and CO_2 isotherms are available; MIL-101(Cr)-PEI-800 shows the highest CO_2 working capacity, but no data were found for the H_2O isotherm in the pressure and temperature ranges of interest. In this work we

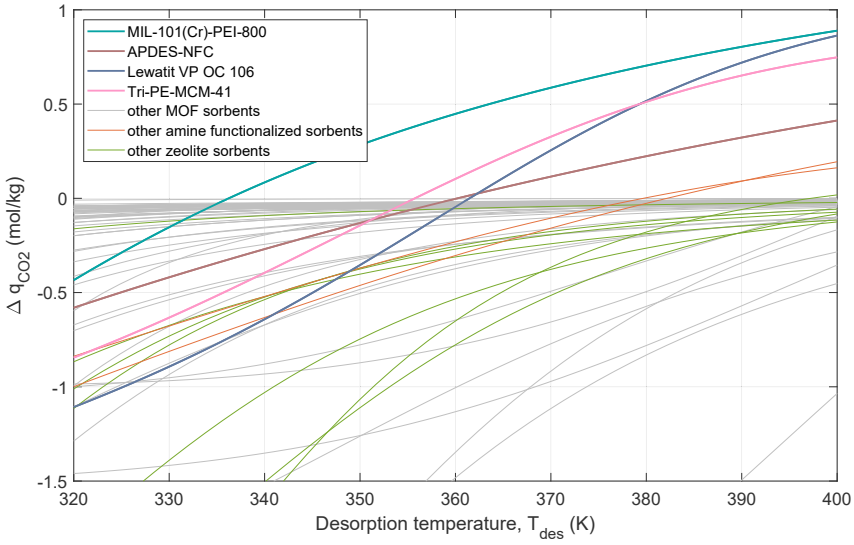

Figure 5. Working capacity for several solid sorbents including zeolites (green lines), MOFs (gray lines), and amines (orange lines)

The capacity is calculated with ambient conditions for the adsorption step (T=293 K, p=1 bar, p_{CO2}=400 ppm) and a desorption pressure of 100 mbar. The four sorbents selected for this study are shown by thick lines and named in the legend.

cope with the limited availability of data for the considered DAC sorbent by combining the sorbent-specific CO_2 isotherm with different H_2O isotherms, which allows us to better evaluate the role of water in the process. To this end we consider the H_2O isotherms of APDES-NFC, Lewatit, and MCF-APS-hi,[58] which feature a high, medium, and low water adsorption, respectively. Moreover, as the current sorbent landscape does not allow us to set a reference sorbent, such as among the four selected, we include in our analysis an exemplary sorbent for CO_2, obtained by combining the equilibrium data of the four materials highlighted in Figure 5. The resulting different cases are listed in Table 1. The matrix of cases obtained in such a fashion allows us to consider sorbents well characterized (APDES-NFC and Lewatit), as well as a promising sorbent missing experimental data (MIL-101(Cr)-PEI-800), and an exemplary sorbent representing the average behavior.

For the four sorbents highlighted in Figure 5, we fitted experimental adsorption data by applying suitable isotherm models. For CO_2 adsorption, we identified two different models that returned the best fitting. For APDES-NFC we apply the temperature-dependent Toth model:

$$q_i(p,T) = \frac{n_s b p_i}{\left(1+(bp_i)^t\right)^{1/t}},\ i = CO_2 \qquad \text{(Equation 8)}$$

For the remaining sorbents we adopted a modified version of the classical Toth equation, where two terms are present, one for describing physisorption and one for describing chemisorption, as proposed by Elfving et al.[59] This model showed the best fitting for three out of four sorbents, since it describes two independent adsorption mechanisms—chemisorption by the amine groups and physisorption by the surface interaction.[60]

$$q_i(p,T) = \left[\frac{n_s b p_i}{\left(1+(bp_i)^t\right)^{1/t}}\right]_{chem} + \left[\frac{n_s b p_i}{\left(1+(bp_i)^t\right)^{1/t}}\right]_{phys} \qquad \text{(Equation 9)}$$

where in both Equations 8 and 9 p_i is the partial pressure of the component i, and n_s, b and t are temperature-dependent parameters of the Toth model. The temperature-dependent coefficients, which have the same functional form for the chemical and the physical term, are defined as follows:

$$n_s(T) = n_{s0}\exp\left[\chi\left(1-\frac{T_0}{T}\right)\right] \qquad \text{(Equation 10)}$$

$$b(T) = b_0\exp\left[\frac{\Delta H}{RT_0}\left(\frac{T_0}{T}-1\right)\right] \qquad \text{(Equation 11)}$$

$$t(T) = t_0 + \alpha\left(1-\frac{T_0}{T}\right) \qquad \text{(Equation 12)}$$

where the terms are as defined in the variable list.[61]

Table 1. Different combinations for CO_2 and H_2O isotherms

CO_2 Isotherm	H_2O Isotherm		
	APDES-NFC	MCF-APS-Hi	Lewatit VP OC 106
APDES-NFC	case 1:A-A	-	-
Exemplary	case 2: **E-A**	case 3: E-M	case 4: **E-L**
MIL-101(Cr)-PEI-800	case 5: MP-A	case 6: MP-M	case 7: **MP-L**
Lewatit VP OC 106	-	-	case 8: **L-L**

The fitting was carried out with the optimization routine *fmincon* in Matlab version R2018b by minimizing the error between the experimental and modeled data using the normalized standard deviation. Further details for the fitting of the different sorbents as well as the calculation of the isosteric heat can be found in the supplemental information. The resulting parameters for the different CO_2 isotherms are shown in Table S2. It can be noted that R-squared is rather high in all cases.

The adsorption isotherms of water were described in all cases by using the Guggenheim-Anderson-de Boer (GAB) model[52,51];

$$q_{H_2O}\left(T, p_{H_2O}\right) = C_m \frac{C_G K_{ads} \frac{p_{H_2O}}{p_0}}{\left(1 - K_{ads}\frac{p_{H_2O}}{p_0}\right)\left(1 + (C_G - 1)K_{ads}\frac{p_{H_2O}}{p_0}\right)} \quad \text{(Equation 13)}$$

with

$$C_G(T) = C_{G,0}\exp\left(\frac{\Delta H_C}{RT}\right) \quad \text{(Equation 14)}$$

$$K_{ads}(T) = K_0\exp\left(\frac{\Delta H_K}{RT}\right) \quad \text{(Equation 15)}$$

$$C_m(T) = C_{m,0}\exp\left(\frac{\beta}{T}\right) \quad \text{(Equation 16)}$$

where the terms are as defined in the variable list. As mentioned before, the equilibrium data of water are from three different sorbents, namely APDES-NFC,[52] MCF-APS-hi,[58] and Lewatit VP OC 106.[62] The resulting parameters for the fitting of the H_2O isotherms are listed in Table S3.

Most of the DAC processes modeled in the literature are either based on dry conditions[60] or disregard the effect of water on the CO_2 isotherm. However, the presence of water in the feedstream enhances the CO_2 capacity of amine-based sorbents, depending on the temperature and partial pressure of H_2O in the stream.[22,34] Despite the very limited set of data available, modeling the cooperative adsorption of water and CO_2 is key to compute a realistic process performance. Ideally, multicomponent competitive isotherms should be used; however, as those are not yet available for the sorbents of interest, we use single component isotherms and describe empirically the interaction of CO_2 and H_2O. Wurzbacher et al.[51] added an enhancing factor dependent on the partial pressure of CO_2 and the humidity, to describe the humid adsorption of CO_2. However, this factor is applicable in a small-pressure range and lead to wrong estimates in other conditions of interest. Using a physical approach, Stampi-Bombelli et al.[41] proposed a new isotherm model for the APDES-NFC sorbent, where the water uptake is embedded in the Toth isotherm for CO_2. This method is physically sound but depends on having comprehensive experimental water isotherms, including competition and cooperative adsorption with CO_2. Here, we applied a robust yet empirical approach by including an equivalent adsorption temperature T_{eq}, which is dependent on the humidity *RH* and the actual temperature *T*, in the form of the following:

$$T_{eq}(T, RH) = T - a\left(\frac{278K}{T}\right)^b RH\,, \quad \text{(Equation 17)}$$

with *a* and *b* being two fitting parameters. The expression allows to have $T_{eq} = T$ for *RH*= 0% whereas also including a minimum T_{eq} for *RH*=100%, such as the most favorable adsorption condition for CO_2 as function of humidity. The calculation of *a* and *b*

was carried out by fitting data provided in Veneman et al.[34] and applied to all sorbents considered in this work. Details can be found in the supplemental information, including the comparison with data reported for APDES-NFC. For the Toth-cp model, the equivalent temperature is included only in the chemisorption, as the physisorption mechanism is not as strongly affected by humidity.

Finally, although we do consider the presence of N_2 in the feed gas and in the void part of the bed, which influences the CO_2 purity, we neglect the adsorption of N_2. It is worth noticing that, given the chemisorption role, the adsorption of N_2 will be very limited.

The adsorption column is simulated by using a deterministic in-house model, which was originally developed for cyclic adsorption processes in fixed beds in the group of Mazzotti at ETH Zurich and that has been adapted here to describe the sorbents of interest. The operation of the process is modeled by solving mass, energy, and momentum balances for a unique column which undergoes the cycle steps sequentially. It is completed when a cyclic steady state (CSS) is reached, or in other words, when the overall mass balance and the internal column parameters, such as composition and temperature, are the same for the n and the $n-1$ cycle. More details can be found in studies conducted by Casas et al., and Joss et al.[63,64] The underlying modeling approach is well established and state-of-the-art in the field of CO_2 adsorption.[65,66] The tool has been validated against experiments for PSA, TSA, and VSA conditions conditions[36,67–69] and has been used in several scientific publications for analysis of adsorption processes.[69–71]

The additional process components, such as the air blower and the vacuum pump, are modeled by using MATLAB. Details can be found in the supplemental information.

Along with the equilibrium data, transport parameters, namely the mass transfer and heat transfer coefficients, are needed. Unfortunately, the data availability for these is even more limited than isotherms. Here, we have tackled this by estimating data from existing experiments, and by adding extensive sensitivity analysis to provide a range of performance, rather than a single-point value. In the adsorption model, the mass transfer resistance is described using the linear driving force (LDF) model;

$$\frac{\partial q_i}{\partial t} = k_i\left(q_i^{eq} - q_i\right) \qquad \text{(Equation 18)}$$

with the (lumped) mass transfer coefficient k_i of component i and the equilibrium adsorbed phase concentration q_i^{eq}. The reference CO_2 coefficient was assumed to be $k_{CO_2} = 0.1\ s^{-1}$, which is in the same range compared with other literature;[72,73] however, other references provide smaller values—e.g., Stampi-Bombelli et al.[41] who fitted the limited set of data from Gebald[42] and Wurzbacher et al.[35,51] resulting in a coefficient of $k_{CO_2} = 0.0002$. Since the kinetics have a large impact on the performance of the process, and given the lack of kinetic data in literature, especially for the specific sorbents we have chosen, a sensitivity analysis is carried out by varying the mass transfer coefficient for CO_2 in the range of $k_{CO_2,1} = 0.0001\ s^{-1}$, $k_{CO_2,2} = 0.01\ s^{-1}$, and $k_{CO_2,3} = 0.1\ s^{-1}$, whereas keeping the kinetics for water constant. Since experimental data provided by Wurzbacher et al.[51] and Cheng et al.[74] showed faster kinetics for H_2O, we assumed $k_{H_2O} = 1\ s^{-1}$ for the mass transfer coefficient.

The heat transfer coefficient was calculated by fitting experimental data provided by Gebald et al.[42]; details of the calculation can be found in the supplemental

information. The resulting coefficient is 6.7 W/(m^{2}K), which is comparable with values used by other authors.[63,75] Since this calculation is only based on one experimental set of data, we included a sensitivity analysis for $h_1 = 4.0$ W/(m^{2}K), $h_2 = 6.7$ W/(m^{2}K) and $h_3 = 10.0$ W/(m^{2}K).

Finally, the specific properties of the different sorbents can be found in Table S4.

Multi-objective optimization

In order to determine the optimal performance of the different capture systems and the associated operating and design variables, a multi-objective optimization was carried out.[76] It includes two competing objectives, namely productivity, which can be seen as an indicator for the resulting equipment costs, and the electrical and thermal energy consumption coupled in the mass-specific exergy e value, which reflects the operating costs. The problem is defined as:

$$\underset{x}{minimize}(-Pr, e) \quad \text{subject to } \Phi \geq \Phi_{spec} \qquad \text{(Equation 19)}$$

where x are decision variables, Φ the purity and Φ_{spec} the required minimum purity (here assumed 95%, as for CO_2 storage applications). Since these objectives are conflicting, the trade-off is identified by a Pareto line; such as for a given reactor size, an increase in productivity requires capturing more CO_2, which can be achieved processing more air (i.e., larger energy consumption for the fan) or working with higher recovery (i.e., larger heat consumption for regeneration). The productivity is calculated as:

$$Pr = \frac{\dot{m}_{CO_2}}{V_{aircontactor}}, \qquad \text{(Equation 20)}$$

where $\dot{m}_{CO_2}$ is the mass rate of CO_2 captured from the air and $V_{aircontactor}$ the volume of the air contactor. The specific exergy requirement e is calculated differently for every process as described below.

Exergy consumption of the alkaline scrubbing process

The specific exergy demand using KOH as a solvent is expressed by:

$$e = \frac{1}{\dot{m}_{CO_2}}\left[\dot{m}_{CH_4} LHV_{CH_4} + \dot{W}_{ASU} + \dot{W}_{blower} + \dot{W}_{comp}\right] \qquad \text{(Equation 21)}$$

where the product $\dot{m}_{CH_4} LHV_{CH_4}$ is the exergy demand for the calcination, which is provided by an oxy-fuel combustion of methane with oxygen from an ASU consuming $\dot{W}_{ASU}$. In addition, the energy requirement for the air blower $\dot{W}_{blower}$ and the compression of the CO_2 $\dot{W}_{comp}$ is included.

Exergy consumption of the MEA scrubbing process

In this case, the exergy demand is calculated as:

$$e = \frac{1}{\dot{m}_{CO_2}}\left[\dot{Q}_{reboiler}\left(1 - \frac{T_0}{T_{reb}}\right) + \dot{W}_{refr} + \dot{W}_{pump} + \dot{W}_{blower} + \dot{W}_{comp}\right] \qquad \text{(Equation 22)}$$

with $\dot{Q}_{reboiler}$ representing the heat required for the reboiler of the stripper, $\dot{W}_{refr}$ the power used for cooling the lean stream and $\dot{W}_{pump}$ the energy requirement of the pumps.

Exergy consumption of the VTSA process

For solid sorbent DAC the specific exergy requirement is calculated as:

$$e = \frac{1}{\dot{m}_{CO_2}}\left[\dot{Q}_{purge}\left(1-\frac{T_0}{T_{purge}}\right)+\dot{Q}_{reg}\left(1-\frac{T_0}{T_{reg}}\right)+\dot{W}_{vac,purge}+\dot{W}_{vac,prod}+\dot{W}_{blower}+\dot{W}_{comp}\right], \quad \text{(Equation 23)}$$

where $\dot{Q}_{purge}$ and $\dot{Q}_{reg}$ represent the heat required for the purge and regeneration step, $\dot{W}_{vac,purge}$ as well as $\dot{W}_{vac,prod}$ the required electrical energy of the vacuum pump, $\dot{W}_{blower}$ the energy for the air blower and $\dot{W}_{comp}$ the energy for CO_2 compression. All input variables are calculated in our optimization framework.

As for the exergy consumption, also the optimization variables are specific to process type.

Optimization variables of the alkali-scrubbing process

- Absorber loading (ξ), defined as the ratio between the moles of KOH in the lean stream and the moles of CO_2 in the air stream;
- Air velocity in the contactor unit (u_{air});
- Mass fraction of water in the K_2CO_3 slurry (w_{H_2O}).

Optimization variables of the MEA scrubbing process

- Absorber loading (ξ), defined in this case as the ratio between the number of moles of MEA in the lean stream and the number of moles CO_2 in the air stream;
- Air velocity in the contactor unit (u_{air});
- Specific reboiler duty (d), defined as the ratio between the set duty of the reboiler and the mass flow rate of the lean stream;
- Split fraction (f_{Split}), the fraction of rich stream, which is directly fed to the top stage of the stripper.

Optimization variables of the VTSA process

- time of the adsorption phase t_{ads}, of the CO_2 production phase t_{prod}, and of the purge step t_{purge};
- vacuum pressure of the preheating and CO_2 production step p_{vac};
- temperature of the heating step T_{prod};
- temperature difference between the CO_2 production and the purge step ΔT_{purge};
- air velocity u_{air} at the feed (the upper boundary is dependent on the specific material properties and is calculated as the minimum fluidizing velocity).

All decision variables and their respective lower and upper boundaries in the optimization are reported in Table S6. The boundaries were chosen to be large enough to explore the optimum for all sorbents, whereas being computationally feasible within some hours.

In all simulations, the optimization is carried out using state-of-the-art mathematical algorithms implemented or available in Matlab (R2018b). For the liquid-scrubbing processes, Matlab was directly connected to Aspen Plus V11 using the ActiveX software framework, so that the data exchange is fully automated. For these cases, the non-dominated sorting genetic algorithm version II (NSGA-II) as available in Matlab was employed. More details can be found in supplemental experimental procedures. For the solid-sorbent process, the optimization was carried out using a new algorithm that (part of) the authors have specifically coded in Matlab for tackling adsorption processes. The algorithm is directly connected to the Fortran-based

adsorption model: it receives results from it and provides new set of optimization variables. The algorithm is a modified version of the global optimization algorithm multi-level coordinate search (MCS), which is extended to deal with multiple objectives (MO-MCS). Details can be found in a publication by Joss et al.[76]

In addition to the objective functions and optimization variables, we report throughout this work also the capture rate. This indicator is defined as the ratio between the amount of CO_2 captured over the amount of CO_2 fed to the air contactor:

$$Cr = \frac{\dot{m}_{CO_2}}{w^{Air}_{CO_2}\dot{m}_{Air}} \quad \text{(Equation 24)}$$

For all processes, the simulations are carried out considering as ambient conditions $T = 293$ K, $p = 1.001$ bar, relative humidity of 43%, and CO_2 content: 4×10^{-4} mol_{CO_2}/mol.

Economic evaluation

As complement to the detailed technical analysis, we carried out a simplified economical evaluation of the different processes. The goal is not to present a detailed economic analysis of the specific technologies, which would require to compute all components of the capital expenditures (CAPEX) and the operational expenditures (OPEX)—out of scope here, but to identify the main cost drivers of the processes and to compare their potential from an economic perspective. In gas separation, energy and air contactor volume are the first proxies for operating and capital cost, respectively. Using the consistent computation of energy performance and productivity we therefore map the CO_2 capture cost c_{CO_2} as function of (i) the air contactor cost per m^3 γ, (ii) the electricity price c_{el}, and (iii) the heat price c_{th}. These can also be regarded as proxy for CAPEX (point (i)) and OPEX (point (ii) and (iii)). The resulting equation is:

$$c_{CO_2} = \frac{\gamma}{Pr \cdot a} + c_{th}e_{th} + c_{el}e_{el}, \quad \text{(Equation 25)}$$

where Pr, e_{th}, and e_{el} are taken from the Pareto fronts computed with the optimization, and a is the lifetime of the plants, which was assumed to be 20 years (note that unit conversion factors have been omitted in the equation). For γ, a range of 2,000 to 50,000 \$/m^3 was chosen. The order of magnitude of the two values has been chosen to cover a broad range of plant costs; from a rather simple and cheap traditional column (as reference a contactor cost of 2,000 $\$/m^3$ was back-calculated from Keith et al.[12]) to the higher cost of a full VTSA system (calculated considering a cost of 600 $\$/ton_{CO_2}$ and the design and capacity of Hinwil Climeworks plant).

For c_{th} and c_{el}, we chose a realistic range of 1–10 \$cents/kWh. It should be stressed that, although we show the full c_{th}-c_{el} plane, cases where heat is more expensive than electricity should be disregarded.

RESULTS AND DISCUSSION

Alkali scrubbing

The Pareto front obtained for the KOH process is reported in Figure 6A. The region below the curve is unfeasible, whereas that above represents a sub-optimal operation.

It is worth noting that the exergy does not change much along the Pareto front, as opposed to the productivity. On the one hand, there is not much room for the reduction of the exergy demand of the KOH scrubbing process with the chosen decision

variables and their respective boundaries. The demand is mainly determined by the oxy combustion, which is around 5 MJ/kg_{CO_2}. A better understanding can be achieved by examining Figure 6B, which shows the breakdown of the exergy demand for the two extremes of the Pareto front. The energy demand is almost equal to the exergy demand, since the calcination is a high temperature process, where energy and exergy converge to the same value.

For both points, the largest share of the exergy demand is due to the calciner and the ASU. The methane and oxygen streams to achieve 98% conversion of $CaCO_3$ at a fixed temperature of 900°C are constant along the Pareto, as a result of the decoupling between the capture and the regeneration sections. As for the purity, the CO_2 concentration in the dried product stream does not differ much from the value of 94.7% and, consequently, the specific energy consumption of the compressors is constant throughout all the simulations.

The energy consumption of the air blowers, on the other hand, significantly changes along the Pareto. As a matter of fact, the pressure drop across the air contactor units increases with increasing air velocity, the latter being one of the design variables chosen for this process.

These results are in line with those presented in the literature. Keith et al. estimate a total exergy demand of 6.57 MJ/kg_{CO_2}, with the calcination representing the largest portion at 5.25 MJ/kg_{CO_2}.[12] The biggest discrepancy can be identified in the CO_2 compression work, as Keith et al. report 0.475 MJ/kg_{CO_2}, whereas, as it is shown in Figure 6B, we estimate 0.34 MJ/kg_{CO_2}. This is likely due to different compressor isentropic efficiencies.

As for the effects of the design variables on the process performance, which are shown in Figure S2, we find that the air velocity has the prominent influence. With increasing air velocity, both the specific energy demand and the productivity

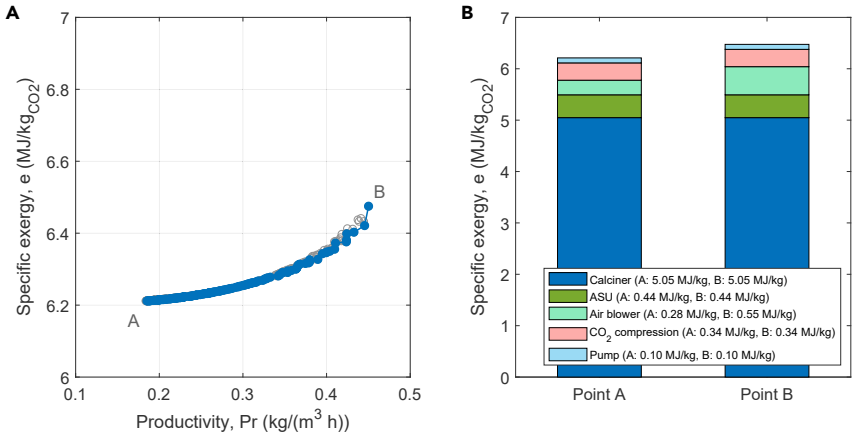

Figure 6. Resulting graphs for the KOH process

(A) Specific exergy-productivity Pareto front for the KOH process; point A: minimum exergy consumption; point B: maximum productivity. Empty points represent sub-optimal conditions obtained during the optimization.

(B) Breakdown of the exergy demand of the alkali-scrubbing process for the two extremes, i.e., point A and B, of the Pareto front. The energy demand is equal to the exergy demand. With the specific values for the calciner A/B: 5.05 MJ/kg, the air separation unit A/B: 0.44 MJ/kg, the air blower A: 0.28 MJ/kg and B: 0.55 MJ/kg, the CO_2 compression A/B: 0.34 MJ/kg and the pumps A/B: 0.10 MJ/kg.

increase, thus delineating the Pareto frontier. Because of the shorter residence time, higher air velocity leads to lower capture rate, which is compensated by the larger amount of CO_2 fed to the contactor. The absorber loading as well as the moisture content of the $CaCO_3$, on the other hand, do not affect the performance significantly. This is a peculiarity of the double ions exchange process, which, from an optimization perspective, allows to decouple the flow rates in the air contactor from the flow rates in the regeneration. Additional details can be found in supplemental experimental procedures.

The purity of the captured CO_2 is independent of the considered design variables and was found to be 94.7% on a dry basis. The remaining impurities consist of N_2, Ar, and O_2 and depend on the ASU and the oxy-combustor design. The CO_2 purity of the alkali-scrubbing process could increase when adopting a gas cleaning process—as done in conventional CCS oxy-combustion processes—or when using an ASU with a third column for Ar recovery. It is in fact worth noting that only negligible amounts of N_2 and Ar are transferred from the air in the air contactor to the regeneration section.

Amine scrubbing

Amine scrubbing is a well-established and widely adopted CO_2 capture process. The DAC version described in this work is based on the unconventional air contactor units of its alkali counterpart, while the solvent regeneration is carried out through conventional steam stripping. The Pareto front for the amine-scrubbing process is reported in Figure 7A.

It can be noted that both productivity and exergy demand change significantly along the Pareto, suggesting the importance of optimization for this process. As for the alkali-scrubbing process, the solvent regeneration is the biggest contributor to the energy demand. Figure 7B shows that, for both extremes of the Pareto, the energy demand consists almost entirely of the reboiler duty. Moreover, it can be noticed that the reboiler duty increases dramatically, when moving toward higher productivity.

Although in terms of exergy demand the amine and alkali-scrubbing processes are similar, amine scrubbing requires much more energy than its alkali counterpart. Figure 7B shows the energy demand for point A of the Pareto, that is the point for which the energy consumption is the lowest. Even in these conditions, the amine-scrubbing process requires almost three times the energy consumed by the alkali process. However, only low-grade heat has to be provided to the reboiler, which explains the significant difference between energy and exergy demand. The results reported in this section are in line with those already published in the literature. However, for operating conditions similar to those adopted in this work, Kiani et al.[19] reported a reboiler duty of 21.9 MJ/kg_{CO_2} and electrical energy requirement of 5.04 MJ/kg_{CO_2}. The energy demand breakdown for point A and B of the Pareto is represented in Figure 7B. The much lower energy requirement of the air blowers reported in this work can be explained by the lower pressure drops provided by the Carbon Engineering-type of air contactor.

The influence of the design variables on the productivity and energy demand is shown in Figure S3. The weight fraction of MEA in the lean stream is kept to the well-established optimal value of 30% throughout all the simulations. This means that an increase in the absorber loading (ξ) determines an increase in the lean flow rate. When moving toward high productivity, both ξ and the air velocity steadily increase. This implies that the lean flow rate is significantly higher, whereas the CO_2 recovered is about constant, thus explaining the rise in energy demand. Remarkably, the specific reboiler duty (d) does not steadily increase as the productivity rises, but it

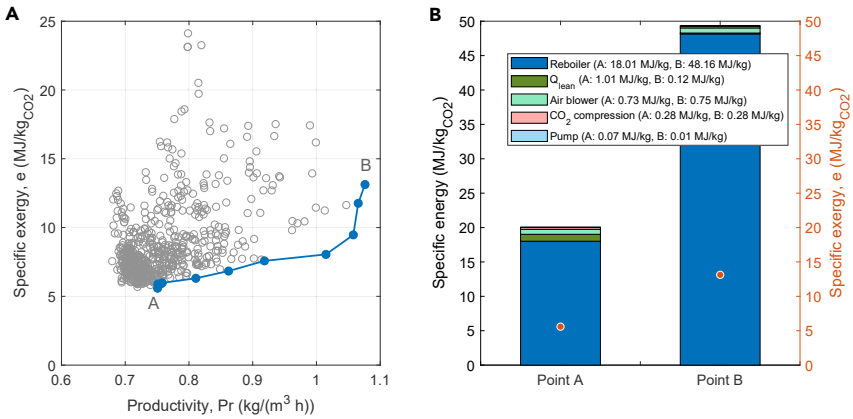

Figure 7. Resulting graphs for the MEA process

(A) Specific exergy - productivity Pareto front for the amine-scrubbing process; point A: minimum exergy consumption; point B: maximum productivity. Empty points represent sub-optimal conditions.

(B) The breakdown of the energy demand for the two extremes, i.e., points A and B, of the Pareto front. With the specific values for the reboiler A: 18.01 MJ/kg and B: 48.16 MJ/kg, the lean stream A: 1.01 MJ/kg and B: 0.12 MJ/kg, the air blower A: 0.73 MJ/kg and B: 0.75 MJ/kg, the CO_2 compression A/B: 0.28 MJ/kg and the pumps A: 0.07 MJ/kg and B: 0.01 MJ/kg. The overall exergy demand for both points is shown by orange dots, using the right axis.

shows a maximum in the middle of the Pareto and then decreases for the points with the highest productivity. This can be explained by the influence of the absorber loading. This design variable increases when moving toward high productivity, meaning that more MEA than CO_2 is present in the system. Therefore, the rich stream becomes more diluted in carbon-carrying components, which affects the energy demand of the reboiler. Indeed, less energy is required to regenerate a more diluted stream, thus the reduction in specific reboiler duty in the high-productivity region. Moreover, less CO_2 is released by regenerating a diluted rich stream; therefore, although *d* decreases, the specific energy demand still increases.

The split fraction does not show a clear trend with respect to the energy demand or the productivity. However, the Pareto points in the high productivity, high energy demand region are all characterized by a high-split fraction, meaning that this design variable does have an effect on the performances of the process.

Interestingly, we show that the kinetic performance of MEA would allow for capturing CO_2 from air. As reported in Figure 8, the capture rate achieved at the Pareto is as high as 89%. The alkali-scrubbing process can provide an even higher capture rate of 97%, although at the expense of productivity. This is due to the fact that higher productivity is achieved via higher air velocity and therefore lower air residence times. In this way more air is processed per time and volume of the reactor. For the highest productivity, the capture rate of the alkali-scrubbing process is 50%. For the amine scrubbing, on the other hand, the capture rate is almost independent of the productivity (i.e., air velocity). This is due to the fast kinetics of MEA, which determine extensive CO_2 removal in the optimal range of the air residence time. Similar performance has also been reported in the recent literature: Barzagli et al.[18] achieved a capture rate of 87.3 %, using an aqueous solution of MEA.

Extremely high CO_2 purities exceeding 97% are achieved. This is not surprising, since MEA is a remarkably selective solvent. The other main components contained in the

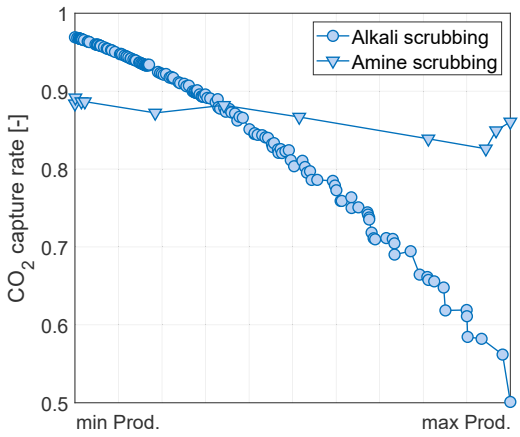

Figure 8. CO_2 capture rate for the resulting Pareto points for both liquid-scrubbing processes over the normalized productivity

CO_2 product stream are H_2O, N_2, and O_2. Thanks to the washing section, the MEA content in the CO_2-lean air stream is negligible. The purity is constant throughout all the operating conditions but tends to slightly decrease with increasing energy demand. An increase in energy demand is determined by a rise in the reboiler duty, meaning that more water is vaporized, partly ending up in the CO_2 stream. However, on a dry basis, the purity achieved with this process is constant.

Solid sorbent

The Pareto curves for the different solid sorbent materials are shown in Figure 9, while the breakdown of the specific exergy and energy consumption can be found in Figure 10. The values for the design variables for each Pareto curve are attached in Figures S5–S12. From Figure 9, it can be noted that the solid-sorbent process covers a rather broad range, both in terms of exergy (1.5–3.7 MJ/kg_{CO_2}) and productivity (3.8–10.6 kg/m^3/h). This is because of the different chemical-physical properties of the sorbents. The highest exergy consumption was achieved with the Lewatit sorbent. One reason is that the heat of adsorption for the chemisorption is 91.2 kJ/mol, which is higher than for the other sorbents and leads to a higher thermal energy demand. Furthermore, the working capacity of the water adsorption is high, which further increases the energy demand during the regeneration step. In addition, the lower particle density and particle diameter limits the maximum air velocity, resulting in a lower productivity. The MIL-101(Cr)-PEI-800 sorbent shows high working capacity and low energy consumption, which depends on the water isotherm. The MFC-APS-hi water isotherm shows the lowest H_2O working capacity and leads to a lower exergy consumption for the combinations using this sorbent, such as MP-M and E-M. For the APDES-NFC sorbent (case A-A), the lower exergy point is comparable with the MIL-101(Cr)-PEI-800 sorbent, but the high productivity is limited to about 6 kg/m^3/h. This is due to the high porosity and low density of the sorbent and the lower working capacity of the CO_2 isotherm, which requires a higher regeneration temperature and a lower vacuum pressure during the production step. For all cases, the main exergy (energy) demand is required by the heat consumption during the regeneration. The energy consumption for the vacuum pump during the purge step is very low, since this step only ensures that all N_2 in the void space is removed to achieve a high purity, which proceeds very quickly. The vacuum pump for the CO_2 production step has a higher share on the overall energy consumption and varies mainly with the different vacuum pressures needed for the regeneration. For the MP-A case, such as the vacuum pressure is comparably high, which results in a very low energy consumption for the pump. The energy consumption for the air blower as well as the CO_2 compression is similar for all cases. The former has a higher impact on the productivity. Whereas keeping the dimensions of the air contactor the same, a higher air velocity leads to an increase in

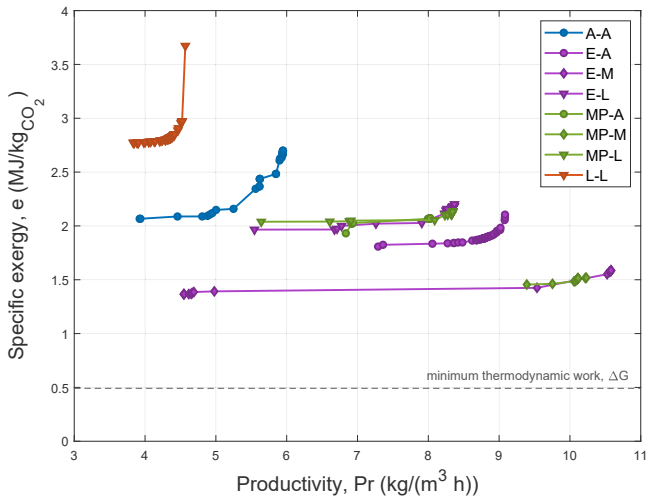

Figure 9. Productivity-exergy Pareto curves for the solid sorbent optimization using different combinations of isotherms for CO_2 and H_2O

In all simulations the mass transfer coefficient for CO_2 is 0.1 $1/s^2$ and the heat transfer coefficient $6.7 W/m^2$. The different colors represent different CO_2 isotherms, while the different symbols change with the different H_2O isotherms.

The shortcuts of the cases are explained in Table 1.

the productivity for the considered range of values. Because of the low temperature of the regeneration, and similarly to MEA, there is a large difference between the energy and exergy demand for all solid sorbents (see Figure 10).

In all cases, the CO_2 purity is in the range of 94% to 99% with water being the main impurity. The only exception is APDES-NFC, where the purity was slightly lower, in the range of 0.89–0.94; this is due to the higher porosity of the sorbent and the additional amount of nitrogen present in the pores. The recovery is similar for all simulations and varies between 60% and 99%, as shown in Figure S4.

Sensitivity analyses were carried out for two highly uncertain parameters: the mass transfer and the heat transfer coefficients. The Pareto fronts for varying the kinetics are shown in Figure 11A. Three cases were analyzed here, depending on their resulting Pareto curves shown in Figure 9, which are: the case with the lowest exergy consumption (E-M), the one with the highest exergy consumption (L-L), and one in between (E-A). It can be noted, that the mass transfer highly affects the shape of the Pareto front. Whereas the minimum energy consumption is similar, the productivity varies significantly when reducing the mass transfer coefficient because of the higher cycle time required. For a specific mass transfer coefficient of $k = 0.1 - 0.01\ s^{-1}$ the Pareto is rather flat - the productivity can be increased with minor additional energy expenditure. However, the Pareto becomes very steep for $k = 0.0001\ s^{-1}$—the productivity can be slightly increased at great energy costs. This effect is similar for all three materials tested. Varying the heat transfer coefficient mainly affects the productivity, such as the lower productivity for smaller heat transfer coefficient, which is due to the longer heating time required as shown in Figure 11B. Differently from the mass transfer, heat transfer does not strongly affect the adsorption step.

For the solid sorbent process, we find that the total energy demand varies in a range of 4.9–13.3 MJ/kg_{CO_2}. The thermal energy is the largest contribution (4 -11.8 MJ/kg), whereas the electrical energy accounts for 0.8–1.8 MJ/kg.

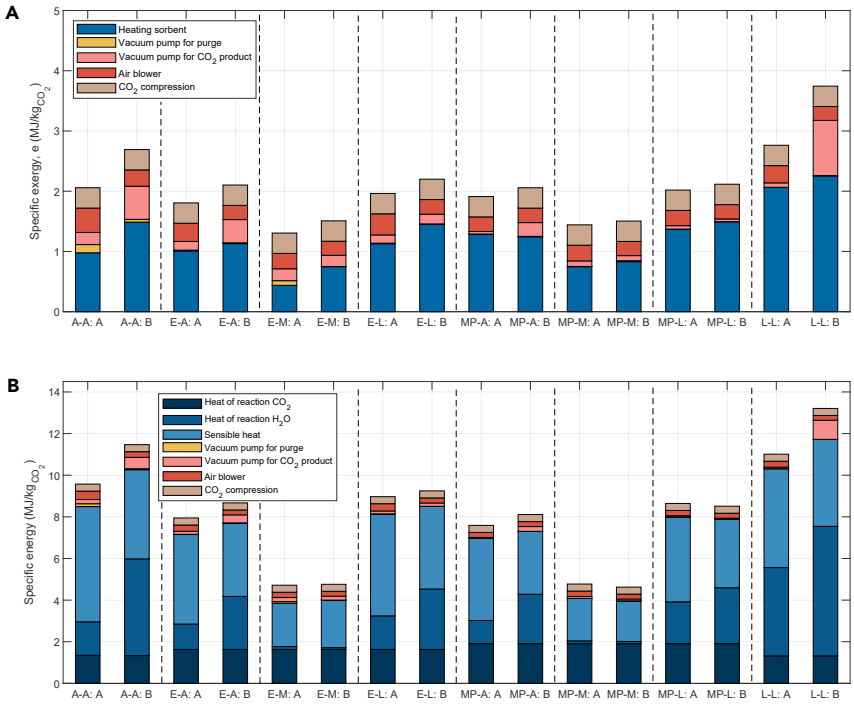

Figure 10. Detailed energy and exergy demand for the different cases of the solid sorbent process

(A) Breakdown of the exergy demand.

(B) Breakdown of the energy demand. The thermal energy demand is shown in blue, with different shades referring to the reaction heat of CO_2 and H_2O, which were calculated at equilibrium (T = 373 K, p = 0.1 bar), and the sensible heat of the sorbent, CO_2 and H_2O. In both graphs X-X:A refers to the minimum exergy/energy on the Pareto, and X-X:B to the maximum productivity.

We can compare the results presented here with values reported in the literature; this is possible for the energy consumption only, as—to the best of our knowledge—no other study reports the CO_2 productivity (or required volume). Moreover, it is worth stressing that different literature works rely often on different assumptions and different sorbents. Finally, the results we present are obtained with an extensive process optimization, whereas literature results are either single data point or outcome of sensitivity analysis.

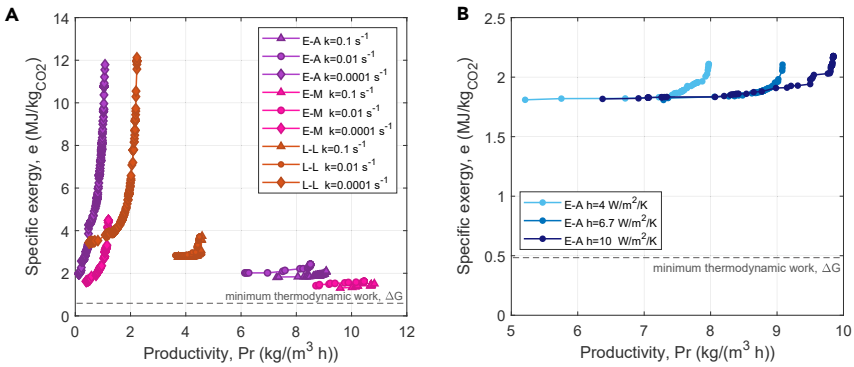

Figure 11. Pareto curves for the sensitivity analysis

(A and B) (A) Changing the kinetics from $k = 0.1 s^{-1}$ to $k = 0.0001 s^{-1}$ (for material E-A, E-M and L-L) and (B) changing the heat transfer coefficient (W/m^2K) (for material E-A).

The process developed by Climeworks requires 1.8–2.6 MJ_{el}/kg and 5.4–11.9 MJ_{th}/kg, where the minimum represents future target and the maximum the current consumption.[77] For our case A-A, which includes the APDES-NFC sorbent supposedly similar to Climeworks material, the energy demand is 1.1–1.3 MJ_{el}/kg and 8.6–10.1 MJ_{th}/kg and therefore in line with published data. As for the electricity consumption, likely sources of deviations include the vacuum pump and blower efficiency, and the pressure drops in the contactor (e.g., we do not account for concentrated pressure drops). As for the heat consumption, the main difference is found when comparing the future Climeworks target, which includes heat integration options between heating and cooling and that we do not include in our models.

Bajamundi et al. report measured data of a modular DAC system using an amine-functionalized polystyrene sorbent, operating as a TVSA cycle. The resulting thermal energy demand is in the area of 27.4 MJ/kg and the mean electrical energy demand is 8.6 MJ/kg.[78] The test was carried out with varying atmospheric temperature and humidity, which is a possible source of higher energy consumption. However, the reported energy consumption is significantly higher than other experimental and numerical studies, which might be linked to the specifics of the experimental plant.

Kulkarni and Sholl report modeling results with an energy requirement of 0.79 MJ_{el}/kg and 6.0 MJ_{th}/kg when using an amino-modified silica adsorbent, TRI-PE-MCM-41.[60] We cannot directly compare these with our results because we did not run specific simulations for TRI-PE-MCM-41—but rather consider it when deriving the exemplary sorbent. In fact, the performance is similar to the exemplary sorbent (namely E-A, E-M, and E-L cases), for which we obtain 0.8–1.0 MJ_{el}/kg and 7.1–7.7 MJ_{th}. Despite a few differences between the system configuration affecting the heat consumption, such as direct steam heating, energy results are similar.

Sinha et al.[39] report modeling result for a TVSA system similar to the system of Kulkarni and Sholl, but using two amino-modified MOFs, MIL-101(Cr)-PEI-800, and mmen-Mg2(dobpdc). The reported total energy demand is 5.11 MJ/kg for the former sorbent and 3.6 MJ/kg for the latter. In our simulations for MIL-101(Cr)-PEI-800, we obtain 4.7–8.9 MJ/kg, depending on the adsorption of water. The key difference here is due to the water adsorption, which is not included in the work of Sinha et al. while it is here: when considering the low capacity water isotherm (i.e.,case MP-M), we obtain a total energy demand of 4.7 MJ/kg, fully in line with Sinha et al.

Yu and Brilman measured experimentally an energy consumption of 6.5 MJ_{th}/kg and 0.6 MJ_{el}/kg using Lewatit in a fixed bed reactor.[79] Our corresponding case (L-L) shows values in the range of 10.1–11.8 MJ_{th}/kg and 0.6–1.3 MJ_{el}/kg. The main difference can be found once again in the water, as the experiments were carried out using a dry feed. We estimate that removing water would decrease the energy consumption of about 3 MJ_{th}/kg (see Figure S1), thus in good agreement with the experimental value of Yu and Brilman.

Finally, we can do a back-of-an-envelope comparison of our productivity with a proximate value for Climeworks Hinwil plant. Considering that the demonstration plant is designed for 2,460 kg/day using 18 modules, whose unit size we estimate to be similar to a cube of 1.5 m side, and assuming 24 h/day operation, we obtain about 1.7 kg/m^3/h, in line with our APDES-NFC case when using low linear driving force. Moreover, when comparing DAC to classical TSA applications for CCS, we see that the productivity decreases of approximately one order of magnitude: from 28-70 kg/m^3/h to 0.5–10 kg/m^3/h.

Overall, the solid sorbent process model shows that the performance of different sorbents, here identified by different CO_2 isotherms and physical properties, are strongly affected by the H_2O isotherms and the heat and mass transfer. Within the limits of physics, it is convenient to design DAC sorbents that (1) limit the water adsorption capacity if the energy is to be minimized, (2) possess a positive CO_2-H_2O cooperative adsorption if the productivity is to be maximized, and, in any case, (3) show low mass transfer resistance.

Processes comparison and economic evaluation

The Pareto curves of all three processes are compared in Figure 12. When using KOH as a solvent the productivity is the lowest and considering the exergy-productivity range of all processes, the exergy does not change much with a change in productivity. The MEA process on the other hand is more sensitive for differences in productivity and the exergy consumption increases very steeply with increasing productivity. The optimization with the solid sorbent process results in the lowest exergy consumption with the highest productivity, however, with the largest uncertainties. Therefore, we have highlighted the results with a blue area encompassing all computed exergy-productivity data. The area starts approximately nearby the KOH/MEA processes but extends to much higher productivity/lower energy consumption ranges. Table 2 lists the share of the energy demand for the different processes; notably the lowest energy demand is obtained for the KOH process.

It is important to stress that here, the calculation of the productivity is based on the largest contributor to the process footprint, such as the air contactor volume; the two liquid-solvent processes do not include the size of additional components such as

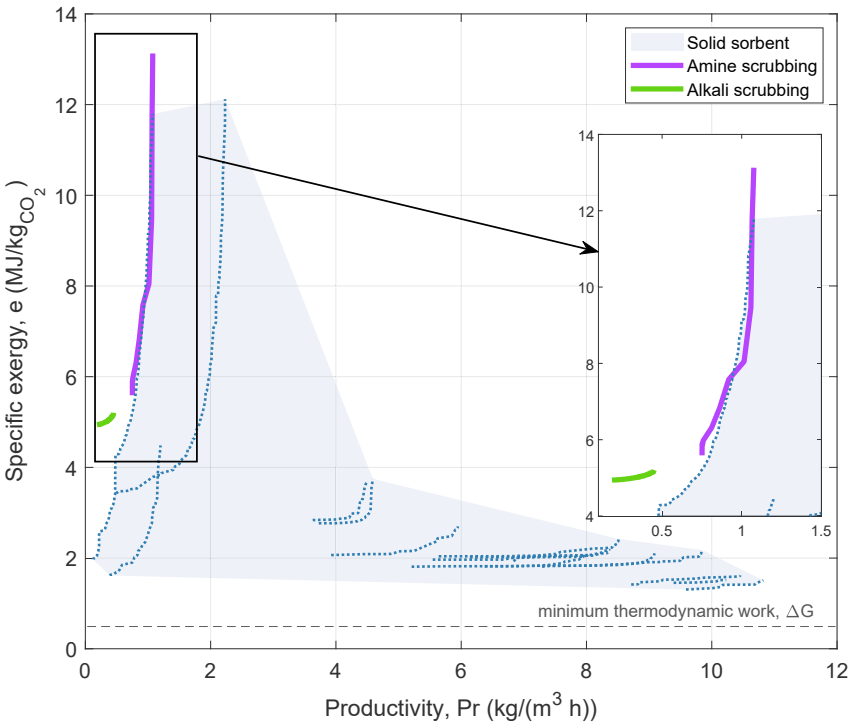

Figure 12. Resulting Pareto charts of all three processes

For the solid sorbent process an area is plotted, which comprises all Pareto plots, including the sensitivity analysis.

the calciner/reboiler or other equipment. Similarly, for the solid sorbent process, we did not consider the size of the piping and valves equipment. We note that by leaving out these ancillary equipment, the productivity calculations are slightly advantageous for the liquid-solvent processes, since the additional components take up more space compared with the solid sorbent process.

The results of the cost analysis are shown in Figure 13, which reports the maps of the total system costs as function of the heat price (c_{th}), the electricity price (c_{el}), as well as the air contactor cost (γ). We find that, for all processes but the solid sorbent with high mass transfer, the cost is strongly dependent on the module cost. Accordingly, low-cost area (<200$\$/ton_{CO2}$) is found for the low range of γ. The MEA economics (Figure 13B) strongly depends on the heat price, since the thermal energy demand is dominating. Accordingly, a low-cost area (<200$\$/ton_{CO2}$) can be found at low heat cost and low module cost. The total costs increase significantly for values of c_{th} above 5 $\$cents/kWh_{th}$, irrespective of the module cost. Compared to the MEA process, the alkali scrubbing (Figure 13A) shows more favorable total costs, which do not depend strongly on the heat price thanks to the significantly smaller thermal energy demand. On the other hand, the low productivity makes the process more dependent on the module cost. The solid sorbent process is shown in Figures 13C and 13D, for low and high mass transfer rates, respectively. For materials allowing high mass transfer rates, the process shows on average the lowest costs thanks to the combination of low energy demand and high productivity compared with the two liquid-solvent processes. In this case, the costs are mainly dependent on the heat price. However, this changes significantly in case of low mass transfer rates as the capture cost becomes strongly dependent on the module cost, with a resulting behavior similar to the MEA, though more favorable.

In this simplified economic calculation, we did not differentiate between high- and low-temperature heat. However, we can reasonably assume that the requirement of low temperatures opens opportunities for recovering low-grade heat, typically wasted, especially if simple heat collection is possible. We can visualize this by using exergy rather than energy for computation of the heat costs; the results are shown in Figure S13. Notably, for the KOH process results stay nearly the same; i.e., there are no opportunities to use waste heat in the calciner, whereas the MEA process becomes much cheaper compared with the previous results. The costs for the solid sorbent process decrease as well.

Overall, from the energy-productivity-costs analysis presented here we can reach the following recommendations:

- For the MEA process (and similar liquid-scrubbing processes using amines as solvents), improvement efforts must be focused on lowering the thermal

Table 2. Energy and exergy consumption of the three processes for the two extreme Pareto points A and B, referring to the Pareto charts shown in Figure 12

	KOH		MEA		Solid sorbent	
	A	B	A	B	A	B
Energy (MJ/kg_{CO_2})	6.21	6.48	20.04	49.32	7.96	8.68
					(3.98–11.17)	(4.69–23.49)
Exergy (MJ/kg_{CO_2})	6.21	6.48	5.59	13.13	1.81	2.1
					(1.31–3.45)	(1.42–12.12)

For the solid sorbent process the exemplary isotherm is considered (case E-A) and the range in brackets indicates the results of the sensitivity analysis.

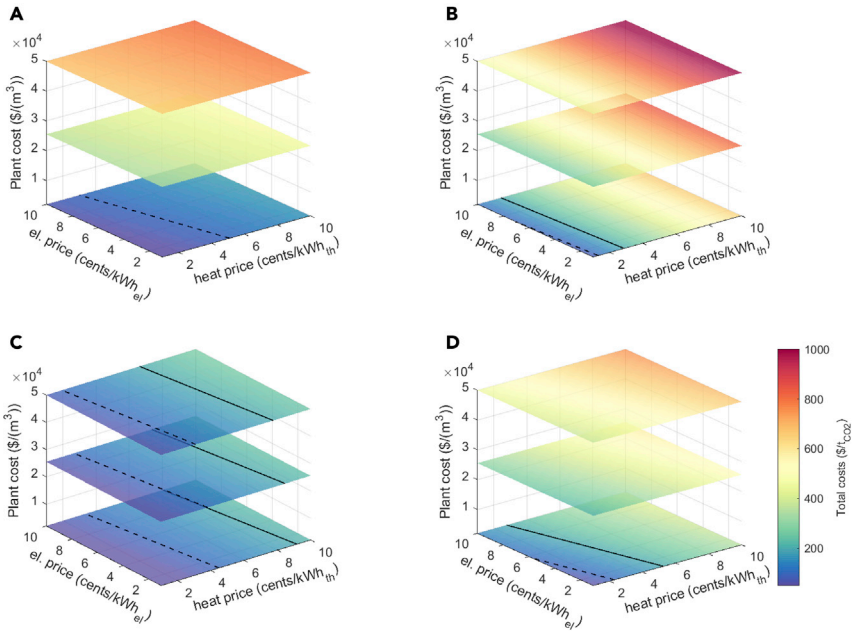

Figure 13. Maps of total system cost as a function of electricity price, heat price, and plant cost, referring to the m^3 of air contactor for the three different processes

(A–D) (A) KOH using point B on the Pareto chart (highest productivity), (B) MEA using point A on Pareto chart (lowest exergy consumption), and (C and D) solid sorbent case E-A (C: high kinetics k = 0.1 s^{-1}using point B on Pareto chart and D: low kinetics k = 0.0001 s^{-1} using a middle point on the Pareto chart with an exergy consumption similar to the KOH process). We have assumed full-load operation plant, a 20-year project life and an 10% discount rate. The dashed lines show total costs with a value of 100 $/$t_{CO2}$ and the continuous lines a value of 200 $/$t_{CO2}$. As an example: when assuming heat costs of c_{th}=5 $cents/$kWh_{th}$, electricity costs of c_{el} = 10 $cents/$kWh_{el}$ and contactor costs of γ = 25,000 $/$m^3$, this would result in total costs of 419 $/$t_{CO2}$, 537 $/$t_{CO2}$, 149 $/$t_{CO2}$ and 427 $/$t_{CO2}$ for the KOH, MEA and the two solid sorbent processes, respectively.

energy consumption, possibly via a combination of more favorable solvents and advanced process configurations, similarly to what has been done in standard CCS applications. Especially, new solvents need to nicely combine high CO_2 loading, fast reactions, limited toxicity, and simple manufacturing. More advanced existing solvents (e.g., the proprietary solvent from MHI, Cansolv, and AkerCCS), are worth testing in DAC applications.

- For the KOH process, it is key to keep the contactor cost low, which is likely possible thanks to the simple design and the use of established components (i.e., contactor packing). The low process productivity and resulting high dependency on contactor costs also call for a simpler regeneration process compared with the current configuration.
- For the solid sorbent process using existing sorbents, the cost optimal design requires to fully characterize the sorbent from a multicomponent equilibrium and transport perspective. Once sorbent characteristics are known, the improvement priority can be either directed on decreasing the contactor costs, such as via additive manufacturing, or on designing a convenient energy system for heat provision, such as via integrating heat recovery options.
- The development of new solid sorbents, which can in principle exploit several thousands of possible new structures,[80] should always prioritize high mass transfer, and should be connected to the environment and application, where DAC is supposed to work. If the productivity is to be prioritized, new sorbents should exploit the cooperative adsorption of CO_2 and H_2O and be designed

for operating in countries with moderate-to-high humidity. If the energy consumption is to be minimized, new sorbents should selectively adsorb CO_2 over H_2O and be designed for operating in arid countries with high renewable heat potential.

When comparing the different technologies, we can note that:

- Productivity: Both liquid-solvent processes show a low productivity range, with [0.18–0.45 kg_{CO_2} m^{-3} h^{-1}] for the alkali scrubbing and [0.75–1.08 kg_{CO_2} m^{-3} h^{-1}] for the amine scrubbing. For the solid sorbent process this range is much broader with [3.8–10.6 kg_{CO_2} m^{-3} h^{-1}], but more data uncertainties are present.
- Energy consumption: The amine scrubbing process shows the highest energy demand, resulting in a 2^{nd} law efficiency of $\eta_{nd} = 3.8 - 8.8\%$. For the KOH process the energy demand is lower, but at high temperature, thus requiring hydrocarbon fuels, resulting in $\eta_{2nd} = 7.6 - 7.9\%$ (the 2^{nd} law efficiency is calculated as the ratio between the exergy obtained here and the minimum thermodynamic work of separation). For the solid sorbent process, the energy consumption is relatively low, and at low temperature, with potential for heat integration with other processes ($\eta_{2nd} = 13.1 - 37.7\%$).
- Scalability: For the liquid-solvent processes, the capture unit is modular and can be easily scaled up and down. Concerning the regeneration, a complex process is required for the alkali scrubbing, which fits better large-scale plants. For the amine scrubbing, the regeneration process is moderately complex, requiring dedicated equipment (heat exchanger, stripper, etc.) and thus would not fit small scales. The solid sorbent process could be easily scaled up and down, but at large scale the piping and the number of valves would make the process design and control challenging. In addition, the process is discontinuous and therefore requires storage vessels (here not considered).
- Economic performance: All three processes have areas of cost lower than 200 $/$t_{CO2}$, but this is achieved for different boundary conditions. MEA benefits the most of low heat price while KOH of low contactor cost. Depending on the specific mass transfer coefficient, solid sorbent benefits of low heat price or low contactor cost. When looking at the contactor cost for the three different processes, it is worth noting that the volume-specific cost for liquid scrubbing is likely lower than for solid sorbents, as conventional packing and cheap solvents are used instead of expensive sorbents (i.e., in Figure 13 the liquid scrubbing are more likely to work in the region of low contactor cost than solid sorbents).
- Fitness for 1.5°C scenario: The solvents for the liquid-scrubbing processes are available at large scale, but the water consumption is high, which would be problematic in water-distressed areas. For the regeneration, the heat provision for the amine scrubbing, as well as the fuel for the alkali-scrubbing process must be CO_2-neutral. For the solid sorbent process, a sorbent for DAC application is not yet available at the scale for capture of$gton_{CO_2}$ per year, and the heat provision must be CO_2-neutral; on the other hand, there is the possibility to co-produce clean water. In all cases, the process must be designed with a system approach that includes the energy provision.
- Scientific challenges: The liquid-solvent processes are already well understood. For the solid sorbent process, there is a lack of experimental data relevant for DAC applications and the underlying adsorption mechanisms are not yet fully understood.

- Technological challenges: A more efficient design of the different reactors of the regeneration section, as well as the electrification of the calciner can further improve the alkali-scrubbing process. Concerning the amine scrubbing, research on the redesign of the absorber for handling more advanced amines (volatility, toxicity, etc.) is needed. Challenging fields for the solid sorbent process comprise the development of an efficient heat exchange within the contactor, heat integration (heating/cooling), an advanced design of the contactor as well as the identification of a leading sorbent.

Conclusions

In this paper, three main DAC processes have been analyzed and their process line-ups optimized. They were subsequently compared on the basis of their exergy and energy demand as well as productivity. The alkali-scrubbing and solid sorbent VTSA processes have been selected because of their comparative technical maturity among the novel DAC processes. For comparison, the conventional and technically mature amine scrubbing process has been added as a benchmark by extending its operating range from flue gas to air capture. These processes have been modeled with state-of-the-art tools and a rigorous multi-objective optimization has been carried out to identify the best design. The results have shown that the absorption-based processes perform generally worse than the solid sorbent process. The productivity for the alkali and amine-scrubbing processes ranges between 0.18 - 0.45 kg_{CO_2} m^{-3} h^{-1} and 0.75 - 1.07 kg_{CO_2} m^{-3} h^{-1}, respectively. For the solid sorbent process it can vary between 3.8 - 10.6 kg_{CO_2} m^{-3} h^{-1}, however, when accounting for the uncertainties surrounding the mass transfer in the adsorption process and including the lowest estimates presented in literature, the productivity range broadens to 0.13–10.6 kg_{CO_2} m^{-3} h^{-1}. The solid VTSA process also comes out on top when we consider exergy demand, which could be as low as 1.31 $MJkg_{CO2}^{-1}$ in the best case and, moreover, of a lower temperature than the one required by the absorption processes. The three technologies have also been compared from an economic point of view. The aim, in this case, was not to provide an accurate cost evaluation, but to compare the economic potential of the processes on the basis of common assumptions. The total cost has been calculated using the productivity and energy demand computed with thermodynamic models, which makes the relative comparison strong, while providing a simple estimate of absolute values. To account for uncertainties and fluctuation in energy prices, the costs have been evaluated for a certain range of electricity, heat, and contactor prices. From this analysis as well the VTSA proves to be the most promising process. Its higher productivity makes its cost less dependent on the air contactor price, which is encouraging, as advanced design of the contactor and novel sorbents could be more expensive than what is currently expected. While the solid sorbent VTSA process comes forward from our analysis has the most attractive option, many questions are yet to be answered to be effectively deployed at large scale, with the most pressing involving the adsorbent itself. The adsorption/desorption kinetics and the affinity of the sorbent for H_2O have a tremendous influence on the performance of the VTSA process, but information on this is scarcely reported in the literature, even for the most prominent materials. Moreover, there are also technological issues to be solved. The sorbent regeneration requires considerable amounts of (low temperature) heat: an optimal air contactor design should allow efficient heat transfer and recovery. We believe that by addressing these challenges the greatest benefits could be reaped. On the other hand, the alkali and amine-scrubbing processes will likely be needed to meet the carbon removal targets consistent with 1.5°C.

EXPERIMENTAL PROCEDURES

Resource availability

Lead contact

Further information and requests for resources and materials should be directed to the lead contact, Matteo Gazzani (m.gazzani@uu.nl).

Materials availability

This study did not generate new unique materials.

Data and code availability

All data used in this paper have been previously published and are available online as referenced throughout the manuscript (e.g., sorbents isotherms data, KOH and MEA reaction rates). Similarly, all codes used in this paper have either been previously published and are described in the references provided (e.g., 1-D VTSA code and VTSA optimization algorithm), or are commercially available (Aspen Plus, MATLAB). For suggestions and tips about the connection between Aspen Plus and MATLAB (or other Windows-based software), which is shortly mentioned in the Aspen Plus user guide, prospective users should contact the lead author, who will be happy to help if possible.

SUPPLEMENTAL INFORMATION

Supplemental information can be found online at https://doi.org/10.1016/j.joule.2021.05.023.

ACKNOWLEDGMENTS

This work was sponsored by Shell Global Solutions International BV.

AUTHOR CONTRIBUTIONS

Conceptualization, M.G. and M.S.A.; methodology, M.G., A.G., and F.S.; software, M.G., F.S., and A.G.; investigation, F.S. and A.G.; writing – original draft, F.S. and A.G.; writing – review & editing, M.G., M.S.A., G.J.K., and F.G.; funding acquisition, M.S.A., G.J.K., and F.G.; resources, M.S.A., G.J.K., and F.G.; supervision, M.S.A., G.J.K., F.G., and M.G.

DECLARATION OF INTERESTS

The authors declare no competing interests.

Received: March 2, 2021
Revised: April 26, 2021
Accepted: May 26, 2021
Published June 24, 2021

REFERENCES

1. Rogelj, J., Shindell, D., Jiang, K., Fifita, S., Forster, P., Ginzburg, V., Handa, C., Kheshgi, H., Kobayashi, S., Kriegler, E., et al. (2018). In Glob. War Med. 1°C. An IPCC Spec. Rep. impacts Glob. Warm, 1.5°C above pre-industrial levels Relat. Glob. Greenh. gas Emiss. pathways, Context Strength. Glob. response to Threat, C. Chang, V. Masson-Delmotte, P. Zhai, H.O. Pörtner, D. Roberts, J. Skea, P. Shukla, A. Pirani, W. Moufouma-Okia, C. Péan, R. Pidcock, S. Connors, J.B.R. Matthews, Y. Chen, X. Zhou, M.I. Gomis, E. Lonnoy, T. Maycock, M. Tignor, and T. Waterfield, eds.

2. Allen, M., Dube, O.P., Solecki, W., Aragón-Durand, F., Cramer, W., Humphreys, S., Kainuma, M., Kala, J., Mahowald, N., Mulugetta, Y., et al. (2018). In Glob. War Med. 1°C. An IPCC Spec. Rep. impacts Glob. Warm, 1.5°C above pre-industrial levels Relat. Glob. Greenh. gas Emiss. pathways, Context Strength. Glob. response to Threat, C. Chang, V. Masson-Delmotte, P. Zhai, H.O. Pörtner, D. Roberts, J. Skea, P. Shukla, A. Pirani, W. Moufouma-Okia, C. Péan, R. Pidcock, S. Connors, J.B.R. Matthews, Y. Chen, X. Zhou, M.I. Gomis, E. Lonnoy, T. Maycock, M. Tignor, and T. Waterfield, eds.

3. Fuss, S., Lamb, W.F., Callaghan, M.W., Hilaire, J., Creutzig, F., Amann, T., Beringer, T., de Oliveira Garcia, W., Hartmann, J., Khanna, T., et al. (2018). Negative emissions—Part 2: Costs, potentials and side effects. Environ. Res. Lett. *13*, 063002.

4. Nemet, G.F., Callaghan, M.W., Creutzig, F., Fuss, S., Hartmann, J., Hilaire, J., Lamb, W.F., Minx, J.C., Rogers, S., and Smith, P. (2018). Negative emissions—Part 3: innovation and upscaling. Environ. Res. Lett. *13*, 063003.

5. Keith, D.W., Heidel, K., and Cherry, R. (2010). Capturing CO2 from the atmosphere: rationale and process design considerations. In Geo-Engineering Climate Change Environmental Necessity or Pandora's Box? (Cambridge University Press), pp. 107–126.

6. Sanz-Pérez, E.S., Murdock, C.R., Didas, S.A., and Jones, C.W. (2016). Direct capture of CO2 from Ambient Air. Chem. Rev. *116*, 11840–11876.

7. Zeman, F.S., and Lackner, K.S. (2004). Capturing carbon dioxide directly from the atmosphere. World Resour. Rev *16*, 157–172.

8. Baciocchi, R., Storti, G., and Mazzotti, M. (2006). Process design and energy requirements for the capture of carbon dioxide from air. Chemical Engineering and Processing: Process Intensification *45*, 1047–1058.

9. Socolow, R., Desmond, M., Aines, R., Blackstock, J., Bolland, O., Kaarsberg, T., Lewis, N., Mazzotti, M., Pfeffer, A., Sawyer, K., et al. (2011). Direct Air Capture of CO2 with Chemicals: A Technology Assessment for the APS Panel on Public Affairs (American Physical Society)).

10. Holmes, G., and Keith, D.W. (2012). An air–liquid contactor for large-scale capture of CO2 from air. Philos. Trans. R. Soc. Lond. A *370*, 4380–4403.

11. Holmes, G., Nold, K., Walsh, T., Heidel, K., Henderson, M.A., Ritchie, J., Klavins, P., Singh, A., and Keith, D.W. (2013). Outdoor prototype results for direct atmospheric capture of carbon dioxide. Energy Procedia *37*, 6079–6095.

12. Keith, D.W., Holmes, G., St Angelo, D., and Heidel, K. (2018). A process for capturing CO2 from the atmosphere. Joule *2*, 1573–1594.

13. Sabatino, F., Mehta, M., Grimm, A., Gazzani, M., Gallucci, F., Kramer, G.J., and van Sint Annaland, M. (2020). Evaluation of a direct air capture process combining wet scrubbing and bipolar membrane electrodialysis. Ind. Eng. Chem. Res. *59*, 7007–7020.

14. Brethomé, F.M., Williams, N.J., Seipp, C.A., Kidder, M.K., and Custelcean, R. (2018). Direct air capture of CO2 via aqueous-phase absorption and crystalline-phase release using concentrated solar power. Nat. Energy *3*, 553–559.

15. Custelcean, R., Williams, N.J., Garrabrant, K.A., Agullo, P., Brethomé, F.M., Martin, H.J., and Kidder, M.K. (2019). Direct air capture of CO 2 with aqueous amino acids and solid bis-iminoguanidines (BIGs). Ind. Eng. Chem. Res. *58*, 23338–23346.

16. Rochelle, G.T. (2009). Amine scrubbing for CO2 capture. Science *325*, 1652–1654.

17. Lackner, K.S. (2009). Capture of carbon dioxide from ambient air. Eur. Phys. J. Spec. Top. *176*, 93–106.

18. Barzagli, F., Giorgi, C., Mani, F., and Peruzzini, M. (2020). Screening study of different amine-based solutions as sorbents for direct CO 2 capture from air. ACS Sustainable Chem. Eng. *8*, 14013–14021.

19. Kiani, A., Jiang, K., and Feron, P. (2020). Techno-economic assessment for CO2 capture from air using a conventional liquid-based absorption process. Front. Energy Res. *8*, 92.

20. Goeppert, A., Czaun, M., Surya Prakash, G.K., and Olah, G.A. (2012). Air as the renewable carbon source of the future: an overview of CO2 capture from the atmosphere. Energy Environ. Sci. *5*, 7833.

21. Eisenberger, P.M., Cohen, R.W., Chichilnisky, G., Eisenberger, N.M., Chance, R.R., and Jones, C.W. (2009). Global warming and carbon-negative technology: prospects for a lower-cost route to a lower-risk atmosphere. Energy Environ. *20*, 973–984.

22. Choi, S., Drese, J.H., and Jones, C.W. (2009). Adsorbent materials for carbon dioxide capture from large anthropogenic point sources. ChemSusChem *2*, 796–854.

23. Didas, S.A., Choi, S., Chaikittisilp, W., and Jones, C.W. (2015). Amine-Oxide Hybrid Materials for CO2 Capture from Ambient Air. Acc. Chem. Res. *48*, 2680–2687.

24. Gebald, C., Repond, N., and Wurzbacher, J.A. (2017). United States Patent application publication US/0203249 A1.

25. Gebald, C., Wurzbacher, J.A., Tingaut, P., and Steinfeld, A. (2013). Stability of amine-functionalized cellulose during temperature-vacuum-swing cycling for CO2 capture from air. Environ. Sci. Technol. *47*, 10063–10070.

26. Fasihi, M., Efimova, O., and Breyer, C. (2019). Techno-economic assessment of CO2 direct air capture plants. J. Clean. Prod. *224*, 957–980.

27. Gebald, C., Piatkowski, N., Ruesch, T., and Wurzbacher, J.A. (2016). Organization WO 2014/170184 al. J. World Intellect. Property.

28. Ping E., Sakwa-novak M., and Eisenberger P. (2018). Global Thermostat Low Cost Direct Air Capture Technology. In International Conference on Negative CO2 Emissions.

29. Bhatt, P.M., Belmabkhout, Y., Cadiau, A., Adil, K., Shekhah, O., Shkurenko, A., Barbour, L.J., and Eddaoudi, M. (2016). A fine-tuned fluorinated MOF addresses the needs for trace CO2 removal and air capture using physisorption. J. Am. Chem. Soc. *138*, 9301–9307.

30. Shekhah, O., Belmabkhout, Y., Chen, Z., Guillerm, V., Cairns, A., Adil, K., and Eddaoudi, M. (2014). Made-to-order metal-organic frameworks for trace carbon dioxide removal and air capture. Nat. Commun. *5*, 4228.

31. Darunte, L.A., Oetomo, A.D., Walton, K.S., Sholl, D.S., and Jones, C.W. (2016). Direct air capture of CO 2 using amine functionalized MIL-101(Cr). ACS Sustainable Chem. Eng. *4*, 5761–5768.

32. McDonald, T.M., Lee, W.R., Mason, J.A., Wiers, B.M., Hong, C.S., and Long, J.R. (2012). Capture of carbon dioxide from air and flue gas in the alkylamine-appended metal-organic framework mmen-Mg2(dobpdc). J. Am. Chem. Soc. *134*, 7056–7065.

33. Belmabkhout, Y., Guillerm, V., and Eddaoudi, M. (2016). Low concentration CO2 capture using physical adsorbents: are metal–organic frameworks becoming the new benchmark materials? Chem. Eng. J. *296*, 386–397.

34. Veneman, R., Frigka, N., Zhao, W., Li, Z., Kersten, S., and Brilman, W. (2015). Adsorption of H2O and CO2 on supported amine sorbents. Int. J. Greenh Gas Control. *41*, 268–275.

35. Wurzbacher, J.A., Gebald, C., Piatkowski, N., and Steinfeld, A. (2012). Concurrent separation of CO2 and H2O from air by a temperature-vacuum swing adsorption/desorption cycle. Environ. Sci. Technol. *46*, 9191–9198.

36. Casas, N., Schell, J., Pini, R., and Mazzotti, M. (2012). Fixed bed adsorption of CO2/H2 mixtures on activated carbon: experiments and modeling. Adsorption *18*, 143–161.

37. Azarabadi, H., and Lackner, K.S. (2019). A sorbent-focused techno-economic analysis of direct air capture. Appl. Energy *250*, 959–975.

38. Deutz, S., and Bardow, A. (2021). Life-cycle assessment of an industrial direct air capture process based on temperature–vacuum swing adsorption. Nat. Energy *6*, 203–213.

39. Sinha, A., Darunte, L.A., Jones, C.W., Realff, M.J., and Kawajiri, Y. (2017). Systems design and economic analysis of direct air capture of CO 2 through temperature vacuum swing adsorption using MIL-101(Cr)-PEI-800 and mmen-Mg 2 (dobpdc) MOF adsorbents. Ind. Eng. Chem. Res. *56*, 750–764.

40. Sinha, A., and Realff, M.J. (2019). A parametric study of the techno-economics of direct CO_2 air capture systems using solid adsorbents. AIChE J. *65*, e16607.

41. Stampi-Bombelli, V., van der Spek, M., and Mazzotti, M. (2020). Analysis of direct capture of CO_2 from ambient air via steam-assisted temperature–vacuum swing adsorption. Adsorption *26*, 1183–1197.

42. Astarita, G. (1963). Absorption of carbon dioxide into alkaline solutions in packed towers. Ind. Eng. Chem. Fund. *2*, 294–297.

43. Mahmoudkhani, M., Heidel, K.R., Ferreira, J.C., Keith, D.W., and Cherry, R.S. (2009). Low energy packed tower and caustic recovery for direct capture of CO2 from air. Energy Procedia *1*, 1535–1542.

44. Pinsent, B.R., and Roughton, F.J. (1956). Trans. Faraday Soc. 47, 263–269.

45. Heidel, K.R., Ritchie, J.A., Kainth, A.P.S., and Keith, D.W. (2014).

46. Danckwerts, P.V. (1979). The reaction of CO2 with ethanolamines. Chem. Eng. Sci. *34*, 443–446.

47. Veltman, K., Singh, B., and Hertwich, E.G. (2010). Human and environmental impact assessment of postcombustion CO2 capture focusing on emissions from amine-based scrubbing solvents to air. Environ. Sci. Technol. *44*, 1496–1502.

48. Le Moullec, Y., Neveux, T., Al Azki, A., Chikukwa, A., and Hoff, K.A. (2014). Process

modifications for solvent-based post-combustion CO_2 capture. Int. J. Greenh. Gas Control *31*, 96–112.

49. Austgen, D.M., Rochelle, G.T., Peng, X., and Chen, C.C. (1989). Model of vapor-liquid equilibria for aqueous acid gas-alkanolamine systems using the electrolyte-NRTL equation. Ind. Eng. Chem. Res. *28*, 1060–1073.

50. Amirkhosrow, M., Pérez-Calvo, J.-F., Gazzani, M., Mazzotti, M., and Nemati Lay, E. (2020). Rigorous rate-based model for CO2 capture via monoethanolamine-based solutions: effect of kinetic models, mass transfer, and holdup correlations on prediction accuracy. Sep. Sci. Technol. *29*, 1–19.

51. Wurzbacher, J.A., Gebald, C., Brunner, S., and Steinfeld, A. (2016). Heat and mass transfer of temperature–vacuum swing desorption for CO2 capture from air. Chem. Eng. J. *283*, 1329–1338.

52. Gebald, C., Wurzbacher, J.A., Borgschulte, A., Zimmermann, T., and Steinfeld, A. (2014). Single-component and binary CO2 and H2O adsorption of amine-functionalized cellulose. Environ. Sci. Technol. *48*, 2497–2504.

53. Gebald, C., Meier, W., Repond, N., Rüesch, T., and Wurzbacher, J.A. (2015). Organization WO 2015/185434 al. J. World Intellect. Property.

54. Wurzbacher, J.A., Repond, N., Rüesch, T., Sauerbeck, S., and Gebald, C. (2018). Organization WO. J. World Intellect. Property, (Al, 60) [Pubmed: 083109].

55. Belmabkhout, Y., Serna-Guerrero, R., and Sayari, A. (2010). Adsorption of CO 2-containing gas mixtures over amine-bearing pore-expanded MCM-41 silica: application for gas purification. Ind. Eng. Chem. Res. *49*, 359–365.

56. Sutanto, S., Dijkstra, J.W., Pieterse, J.A.Z., Boon, J., Hauwert, P., and Brilman, D.W.F. (2017). CO 2 removal from biogas with supported amine sorbents: first technical evaluation based on experimental data. Sep. Purif. Technol. *184*, 12–25.

57. Bos, M.J., Kreuger, T., Kersten, S.R.A., and Brilman, D.W.F. (2019). Study on transport phenomena and intrinsic kinetics for CO2 adsorption in solid amine sorbent. Chem. Eng. J. *377*.

58. Didas, S.A., Kulkarni, A.R., Sholl, D.S., and Jones, C.W. (2012). Role of amine structure on carbon dioxide adsorption from ultradilute gas streams such as ambient air. ChemSusChem *5*, 2058–2064.

59. Elfving, J., Bajamundi, C., Kauppinen, J., and Sainio, T. (2017). Modelling of equilibrium working capacity of PSA, TSA and TVSA processes for CO 2 adsorption under direct air capture conditions. J. CO2 Util. *22*, 270–277.

60. Kulkarni, A.R., and Sholl, D.S. (2012). Analysis of equilibrium-based TSA processes for direct capture of CO 2 from air. Ind. Eng. Chem. Res. *51*, 8631–8645.

61. Do, D.D. (1998). Adsorption Analysis: Equilibria and Kinetics: Series on Chemical Engineering (Imperial College Press).

62. García Martínez, J.B. (2020). Study of water adsorption on an amine adsorbent for Direct Air Capture of CO_2. Master thesis (Twente University).

63. Casas, N., Schell, J., Blom, R., and Mazzotti, M. (2013). MOF and UiO-67/MCM-41 adsorbents for pre-combustion CO2 capture by PSA: breakthrough experiments and process design. Sep. Purif. Technol. *112*, 34–48.

64. Joss, L., Gazzani, M., Hefti, M., Marx, D., and Mazzotti, M. (2015). Temperature swing adsorption for the recovery of the heavy component: an equilibrium-based shortcut model. Ind. Eng. Chem. Res. *54*, 3027–3038.

65. Haghpanah, R., Majumder, A., Nilam, R., Rajendran, A., Farooq, S., Karimi, I.A., and Amanullah, M. (2013). Multiobjective optimization of a four-step adsorption process for postcombustion CO 2 capture via finite volume simulation. Ind. Eng. Chem. Res. *52*, 4249–4265.

66. Dantas, T.L.P., Luna, F.M.T., Silva, I.J., de Azevedo, D.C.S., Grande, C.A., Rodrigues, A.E., and Moreira, R.F.P.M. (2011). Carbon dioxide–nitrogen separation through adsorption on activated carbon in a fixed bed. Chem. Eng. J. *169*, 11–19.

67. Streb, A., and Mazzotti, M. (2021). Adsorption for efficient low carbon hydrogen production: part 1—adsorption equilibrium and breakthrough studies for H2/CO2/CH4 on zeolite 13X. Adsorption *27*, 541–558.

68. Marx, D., Joss, L., Hefti, M., and Mazzotti, M. (2016). Temperature swing adsorption for postcombustion CO_2 capture: single- and multicolumn experiments and simulations. Ind. Eng. Chem. Res. *55*, 1401–1412.

69. Marx, D., Joss, L., Hefti, M., Gazzani, M., and Mazzotti, M. (2015). CO_2 capture from a binary CO_2 /N_2 and a ternary CO_2/N_2/H_2 mixture by PSA: experiments and predictions. Ind. Eng. Chem. Res. *54*, 6035–6045.

70. Joss, L., Hefti, M., Bjelobrk, Z., and Mazzotti, M. (2017). On the potential of phase-change adsorbents for CO2 capture by temperature swing adsorption. Energy Procedia *114*, 2271–2278.

71. Streb, A., Hefti, M., Gazzani, M., and Mazzotti, M. (2019). Novel adsorption process for co-production of hydrogen and CO_2 from a multicomponent stream. Ind. Eng. Chem. Res. *58*, 17489–17506.

72. Belmabkhout, Y., and Sayari, A. (2009). Effect of pore expansion and amine functionalization of mesoporous silica on CO2 adsorption over a wide range of conditions. Adsorption *15*, 318–328.

73. Serna-Guerrero, R., Belmabkhout, Y., and Sayari, A. (2010). Modeling CO2 adsorption on amine-functionalized mesoporous silica: 1. A semi-empirical equilibrium model. Chem. Eng. J. *161*, 173–181.

74. Ng, Y.C., Yang, L., and Jovanovic, Z.R. (2018). The development and validation of a closed-loop experimental setup for investigating CO_2 and H_2O coadsorption kinetics under conditions relevant to direct air capture. Ind. Eng. Chem. Res. *57*, 13987–13998.

75. Rajagopalan, A.K., and Rajendran, A. (2018). The effect of nitrogen adsorption on vacuum swing adsorption based post-combustion CO2 capture. Int. J. Greenhouse Gas Control *78*, 437–447.

76. Joss, L., Capra, F., Gazzani, M., Mazzotti, M., and Martelli, E. (2016). MO-MCS: An efficient multi-objective optimization algorithm for the optimization of temperature/pressure swing adsorption cycles. Comput. Aided Chem. Eng. *38*, 1467–1472.

77. Deutz, S., and Bardow, A. (2021a). Life-cycle assessment of an industrial direct air capture process based on temperature–vacuum swing adsorption. Nat. Energy *6*, 203–213.

78. Bajamundi, C.J.E., Koponen, J., Ruuskanen, V., Elfving, J., Kosonen, A., Kauppinen, J., and Ahola, J. (2019). Capturing CO2 from air: technical performance and process control improvement. J. CO2 Util. *30*, 232–239.

79. Yu Q., Brilman D.W.F. Design Strategy for CO_2 Adsorption from Ambient Air Using a Supported Amine Based Sorbent in a Fixed Bed Reactor. Energy Procedia 114;6102–6114.

80. Deeg, K.S., Damasceno Borges, D., Ongari, D., Rampal, N., Talirz, L., Yakutovich, A.V., Huck, J.M., and Smit, B. (2020). In silico discovery of covalent organic frameworks for carbon capture. ACS Appl. Mater. Interfaces *12*, 21559–21568.